Topological data analysis for revealing dynamic brain reconfiguration in MEG data

Ali Nabi Duman [Corresp., 1], **Ahmet E Tatar** [2]

[1] Department of Mathematics, King Fahd University of Petroleum and Minerals, Dhahran, Saudi Arabia

[2] Center for Information Technology, University of Groningen, Groningen, Netherlands

Corresponding Author: Ali Nabi Duman
Email address: aliduman@kfupm.edu.sa

In recent years, the focus of the functional connectivity community has shifted from stationary approaches to the ones that include temporal dynamics. Especially, non-invasive electrophysiological data (magnetoencephalography/electroencephalography (MEG/EEG)) with high temporal resolution and good spatial coverage have made it possible to measure the fast alterations in the neural activity in the brain during ongoing cognition. In this paper, we analyze dynamic brain reconfiguration using MEG images collected from subjects during the rest and the cognitive tasks. Our proposed topological data analysis method, called Mapper, produces biomarkers that differentiate cognitive tasks without prior spatial and temporal collapse of the data. The suggested method provides an interactive visualization of the rapid fluctuations in electrophysiological data during motor and cognitive tasks; hence, it has the potential to extract clinically relevant information at an individual level without temporal and spatial collapse.

Topological Data Analysis for Revealing Dynamic Brain Reconfiguration in MEG Data

Ali Nabi Duman[1] **and Ahmet Emin Tatar**[2]

[1]**Department of Mathematics, King Fahd University of Petroleum and Minerals, Dhahran, Saudi Arabia**
[2]**Center for Information Technology, University of Groningen, Groningen, The Netherlands**

Corresponding author:
Ali Nabi Duman[1]

Email address: aliduman@kfupm.edu.sa

ABSTRACT

In recent years, the focus of the functional connectivity community has shifted from stationary approaches to the ones that include temporal dynamics. Especially, non-invasive electrophysiological data (magnetoencephalography/electroencephalography (MEG/EEG)) with high temporal resolution and good spatial coverage have made it possible to measure the fast alterations in the neural activity in the brain during ongoing cognition. In this paper, we analyze dynamic brain reconfiguration using MEG images collected from subjects during the rest and the cognitive tasks. Our proposed topological data analysis method, called Mapper, produces biomarkers that differentiate cognitive tasks without prior spatial and temporal collapse of the data. The suggested method provides an interactive visualization of the rapid fluctuations in electrophysiological data during motor and cognitive tasks; hence, it has the potential to extract clinically relevant information at an individual level without temporal and spatial collapse.

INTRODUCTION

The functional connectivity studies focusing on the co-activation of spatially separated brain regions have been shown to be fruitful in identifying special features of neural connectivity during resting state and cognitive tasks Bastos and Schoffelen (2016); O'Neill et al. (2015); Friston (2011). These results open the way for using functional connectivity as a biomarker for clinical diagnosis which, for example, measures illness severity Brookes et al. (2016) and predicts the response to clinical intervention Carbo et al. (2017). Despite their success, most of these methods neglect the temporal variations during neural processes Sporns (2013); Hutchison et al. (2013). Time-resolved approaches, on the other hand, can provide a crucial understanding of how the information is processed in the brain as functional connectivity may alter within several hundred milliseconds of a cognitive experiment Smith et al. (2012); Chang and Glover (2010); Tagliazucchi et al. (2012); Antonakakis et al. (2020).

The most common neuroimaging modality to study dynamic functional connectivity has so far been functional Magnetic Resonance Imaging (fMRI). However, it is a challenge to monitor the rapid changes in network dynamics within a short time interval using fMRI, as it only detects a proxy of neuronal activity (i.e. hemodynamic signals) in the brain. In this case, the most reasonable time required to calculate connectivity is 30 s Allen et al. (2012). On the other hand, electrophysiological modalities (i.e. ECoG, EEG, MEG) address this issue with their high temporal resolution and decent spatial scales. Recently introduced non-invasive electrophysiological techniques de Pasquale et al. (2010); Liu et al. (2010) enable us to explore the variations in connectivity dynamics which eventually leads us to the determination of biomarkers in clinical applications.

The sliding window method is a simple and common approach for measuring dynamic connectivity in electrophysiological modalities as it is compatible with most of the static connectivity measures Brovelli et al. (2017); O'Neill et al. (2015, 2017); Carbo et al. (2017); Lee et al. (2017); de Pasquale et al. (2010); Doron et al. (2012); Bassett et al. (2011); Antonakakis et al. (2020). In this approach, the connectivity is assessed over the time windows of a fixed width which are shifted by a fixed step

from the beginning to the end of the experiment. The main limitation with this approach is choosing the window length: While the results with a short window width are affected by noise, the ones with a long window width ignore the rapid fluctuations in the connectivity. Moreover, a fixed window width is not appropriate for the experiments with varying timescales of fluctuation. Hidden Markov Models (HMM) address this issue by measuring the connectivity of the data over aggregated intervals corresponding to certain states, which are characterized by the properties of the source level signal Baker et al. (2014); Vidaurre et al. (2016). A limitation of this method is scalability in the case of a high number of time points and subjects. It is also more suitable to apply to a small number of regions at a time due to possible overfitting resulting from a large number of regions Vidaurre et al. (2018). Examination of microstates in resting-state or during task is another well-established method of analyzing temporal brain activity. Microstates are a series of time intervals during which the scalp potential field's configuration is quasi-stable Michel and Koenig (2018),Khanna et al. (2015),Milz et al. (2016). Similar to other discrete methods, microstate analysis collapses the signals on the time scale losing the possibly valuable information related to the high temporal resolution of MEG data. Different brain patterns might result in the same microstates as the inverse of the microstates are not unique.The effectiveness of these discrete approaches to quantify the brain dynamics is still under discussion among the functional connectivity community Preti et al. (2017). An alternative to avoid the discretization on the temporal scale is the high temporal measures of connectivity exploiting wavelet transform Dhamala et al. (2008) or Hilbert transform Breakspear (2002). Although the high temporal measures are applicable to individual data and capture the connectivity instantaneously, they require averaging, for example, over the trials of the task to increase robustness. Collapsing or averaging the data in time or space makes it difficult to derive the complete picture of how the brain connectivity continuously evolves during rest and task Saggar et al. (2018). To improve translational outcomes, it is important to explore new computational methods that avoid averaging data across individuals, time, or space.

The use of Artificial Neural Networks (ANN) in scientific studies has been increased in recent years Chiniforooshan Esfahani (2023). This trend can also be noticed in brain dynamics research. Deep neural network models are used to improve electrophysiological source imaging of spatiotemporal brain dynamics Sun et al. (2022).Physics-informed neural networks are applied to investigate molecular transport in the human brain using MRI images Zapf et al. (2022) and to provide high-resolution maps of velocity, area, and pressure in the entire brain vasculature from Transcranial Doppler ultrasound data Sarabian et al. (2022). Various graph neural network architectures designed to forecast brain activity based on models of spatiotemporal brain dynamics are compared in Wein et al. (2022). Recurrent Neural Networks are used to predict feature-evoked response sequences from fMRI data Güçlü and van Gerven (2017).The new MEG datasets are also emerging to train and test brain-based ANN models. For example, a narrative comprehension MEG data representing rich variety of temporal dynamics is provided to test ANN based current natural language processing models against brain data Armeni et al. (2022). ANNs have recently been utilized to improve disease diagnosis and classification. Deep neural networks using resting state EEG data of elderly individuals is proposed as a diagnosis tool for preclinical Alzheimer's disease Park et al. (2022). Attention deficit and hyperactivity disorder (ADHD) classification with EEG and ANNs is studied in Martínez González et al. (2022).Another recent application is the detection of Parkinson's disease through resting-state EEG based deep neural networks Shaban and Amara (2022). While ANNs are black-box tools with high accuracy for classification and prediction, their results are hard to interpret due to the complex underlying algorithms. More interactive and inherently interpretable tools are necessary for clinical use.

To address the above issues, we utilize a topological data analysis (TDA) technique called Mapper Singh et al. (2007); Carlsson (2014) using MEG data from Human Connectome Project Larson-Prior et al. (2013). Due to its low sensitivity to noise and coordinate and deformation invariance features, the mathematical graph obtained from Mapper for each subject's MEG data can be visually and graph-theoretically explored making it accessible for clinical use.

Mapper has previously been applied to longitudinal MRI revealing two large subgroups within the population ($n = 52$) of children diagnosed with Fragile X syndrome. Mapper is shown to be promising in brain dynamics analysis for fMRI on an individual level ($n = 1$) making it valuable for translational studies. The mesoscale graph invariants (i.e. modularity and core-periphery) of the output mathematical graph representation not only predict task performance but also differentiates the time points during evoked tasks and resting state by locating them at the core and periphery of the Mapper graph, respectively Saggar et al.

(2018). In a succeeding work, new Python-based interactive visualization tools are provided to examine Mapper graphs Geniesse et al. (2019). Limitations of Mapper such as the need of dimensionality reduction and exploration of vast parameter space are addressed via NeuMapper framework in Geniesse et al. (2022). Mapper has detected a transition state of the brain between different neural configuration from resting-state fMRI data Saggar et al. (2022b). In another work, Mapper has provided an evidence that A greater differential engagement of brain activity was achieved using methylphenidate during an n-back working memory fMRI task Saggar et al. (2022a).In Zhang et al. (2023), dynamical systems features are extracted from Mapper graphs to bridge the gap between data-driven models and mechanistic dynamical systems models.

Here, we apply the Mapper algorithm to the temporal dimension of MEG data, which, unlike fMRI, provides direct measurement of whole-brain activity with richer temporal information. The mesoscale graph invariants of the Mapper graph are shown to be effective in differentiating data collected during working memory, story/math, and sensor-motor experimental paradigms. When these paradigms are compared pairwise, it is found that

- the centrality scores of the working memory task are significantly higher than the centrality scores of the story/math task;
- the centrality scores of the sensory-motor task are significantly higher than the centrality scores of the story/math task;
- there is no significant difference between the centrality scores of the sensory-motor task and the centrality scores of the working memory task;

pointing out the high stability in the temporal brain functional during the high demanding tasks. These results partially agree with the fMRI results Saggar et al. (2018). Additionally, for the working memory and the story/math tasks where the performance is measured and timed, it is shown that there is weak negative and non-significant correlation between the community structure of the graph and the response time. A stronger but statistically weak correlation is also noticed in the fMRI study Saggar et al. (2018). In summary, Mapper provides an interactive visualization of the rapid fluctuations in electrophysiological data during rest and cognitive tasks; hence, it has the potential to extract clinically relevant information at an individual level without temporal and spatial collapse.

METHODS

Ethics Statement

This paper utilised data collected for the HCP Van Essen et al. (2012). The scanning protocol, participant recruitment procedures, and informed written consent forms, including consent to share deidentified data, were approved by the Washington University institutional review board Van Essen et al. (2012). IRB approval number is FEB-20220810-13614

Subjects and Data

The data we use in this research is the human non-invasive resting state and task Magnetoencephalography (MEG) data set which is publicly available from the Human Connectome Project (HCP) consortium Larson-Prior et al. (2013). It is acquired on a Magnes 3600 MEG (4D NeuroImaging, San Diego, USA) with 248 magnetometers and 23 reference channels at the sampling rate of 2034.5101 Hz. The data is available for a total of 100 subjects each performing three experimental paradigms; *Sensory-motor*, *Working memory*, and *Story/Math*.

The tasks in the sensory-motor paradigm involve the execution of a simple hand or foot movement. Which limb on which side is instructed by a visual cue, which serves to pace the movement. The Working memory paradigm is similar or identical to the corresponding task acquired during fMRI imaging of HCP. Here, the participants have to remember the occurrence of n-back previously shown item (with $n = 0$ and $n = 2$) with the items being either tools or faces. Data are segmented to the onset of the non-target item (WM task). The story/math paradigm is the same as that is used in the fMRI component of the HCP Barch et al. (2013). Participants listen either to auditory narratives of around 30 seconds duration or matched-duration simple arithmetic problems followed by a 2-alternative forced choice question Binder et al. (2011). Subjects respond by right-hand button press (index or middle finger).

For every subject, all the paradigms consist of two experimental runs. A run consists of blocks of tasks, a block consists of several trials of the same task with a fixation period between the trials, and finally, a trial consists of a baseline and a stimulus. We shall also note that not all data is available for each Subject.

For a single subject, the data acquired by Magnes 3600 MEG is processed as follows:

- Noisy channels with a high variance ratio and correlation to neighboring channels are detected and removed from further analysis.
- The bad channels and segments are removed with iterative independent component analysis (ICA) using spatial and temporal criteria Mantini et al. (2011).
- Using ICA, independent components (ICs) are classified as 'Brain' or 'Noise' using six parameters: correlation between IC signals, the correlation between power time courses, the correlation between spectra, and three additional parameters derived from both spectral and temporal properties. Physiological artifacts are identified as magneto- and electro-cardiogram, eye movements, power supply bursting, and $1/f$-like environmental noise. The details of this step can be found in Larson-Prior et al. (2013); Mantini et al. (2011).

We note here two of its stages that are related to our preprocessing explained in the next section. First, the sampling rate is lowered to 506.6275, and second, the data from noisy channels are removed. As a result, the time points are reduced by 25% and the channels across the two runs might not be identical.

Preprocessing

We process the data further per subject and per paradigm. We lower the sampling rate down to 256 Hz. We remove all the time points corresponding to the fixation trials and the baseline keeping only the stimulus ones as well as the time points with missing values. Moreover, to concatenate the data from the two runs, we also remove the non-common channels across the runs. As a result, a subject for a given paradigm is represented by a matrix of the form (# channels)$\times$(# time points). The number of channels is changing between 200 to 248 depending on the subject, and the number of time points is ranging between 350,000 and 400,000.

At this point of the preprocessing, each subject is associated with three matrices, one for every experimental paradigm. As we want to compare the paradigms pairwise, in the next stage we concatenate these matrices two by two. This way, each subject is still associated with three matrices corresponding to the cases:

- Working memory and story/math;
- Working memory and sensory-motor;
- Story/math and sensory-motor.

These matrices are concatenated in the above order across the common channels in the paradigms. Even though the concatenation results in the loss of some channels, the loss is not significant and the resulting concatenated matrix has still 200 to 250 channels. In the meantime, the number of time points in the concatenated matrix is almost doubled and ranges between 700,000 and 800,000. In the end, the concatenated matrix is transposed so that the time points are on the vertical axis and the channels are on the horizontal axis.

Finally, we note that this vectorization of the MEG images causes the loss of the locations of channels relative to each other. However, it is shown in various studies that this process does not affect the success of the machine learning methods Bray et al. (2009).

Topological Data Analysis: Mapper

Most of the network neuroscience studies utilize simple graphs focusing on dyadic connection ignoring higher-order interactions that could be crucial to extract insight across multiple scales Torres et al. (2021). The existence, quantification, and comparison of these higher-order interactions necessitate the use of more advanced mathematical structures that can be studied by topological data analysis(TDA), which uses techniques from algebraic topology and computer science to analyze data sets Centeno et al. (2022).

Analysis of these non-dyadic relations makes it possible to deal with the open problems in network neuroscience Andjelković et al. (2020); Billings et al. (2021); Guo et al. (2021); Helm et al. (2021); Patania et al. (2019); Santos et al. (2019); Saggar et al. (2018).

In our study, we adopt a TDA method called Mapper, which is a successful structure discovery and visualization technique for the exploration of high-dimensional data. The resulting mathematical graph from Mapper is a highly compact representation of the complex data revealing insightful coordinate-free visualization. Introduced in 2007 Singh et al. (2007), its application to biological data sets includes but is not limited to disease association, RNA folding, viral evolution, and immunology Chan et al. (2013); Nielson et al. (2015); Li et al. (2015). Hence, its application to brain dynamics is promising as shown in the earlier studies Geniesse et al. (2022, 2019); Saggar et al. (2018); Patania et al. (2019).

The construction of a Mapper graph from a point cloud is illustrated in Fig 1: (i) The first step is the choice of a *filter* which assigns one (or more) values to each data point in the point cloud. The filter values can be height, coordinate values, a measure of centrality, or output of any data mining algorithm such as PCA, SVD, SNE, etc. . (ii) The next step is to cover all possible filter values with overlapping intervals (or regions depending on the dimension of the filter). Three color-coded intervals covering the range of the height function are shown in Fig 1. (iii) Next, the points whose filter values fall in the same interval (or region) clustered using a clustering algorithm such as hierarchical clustering, k-nearest neighbor (KNN), single linkage clustering. For clustering, one can use any metric including correlation, Euclidean, L_1 or L_∞ metrics. (iv) The nodes representing the clusters are finally connected by an edge if the underlying clusters have a non-empty intersection.

The parameters of the algorithm are the number of intervals (or regions), the overlapping percentage, the distance metric, and the clustering algorithm. A high number of intervals increases the number of nodes in the final visualization; hence, defeats the purpose of having a highly compact representation. While an increase in the overlapping percentage results in a high number of edges and increases complexity, a low overlapping percentage produces disconnected clusters and misses the information about variation in the data due to underlying continuous filter values.

We apply the Mapper algorithm to the MEG data from HCP. We use the open source KeplerMapper Python package Veen et al. (2019) to generate Mapper graphs from the minimally processed data. Our goal is to trace the brain activation patterns of each participant during working memory, story/math, and motor tasks. As explained above, the data is concatenated pairwise before entering the Mapper algorithm. It is not uncommon to use concatenated data to estimate task-state functional connectivity and brain networks Richiardi et al. (2011); Hsu et al. (2014); Freeman et al. (2011); Liu et al. (2014); Mokhtari and Hossein-Zadeh (2013); Zhu et al. (2017). Moreover, comparative studies show that functional connectivity for the concatenated data was both qualitatively and quantitatively similar to that of continuous data during rest Fair et al. (2007); Gavrilescu et al. (2008); Cheng et al. (2015) and task Zhu et al. (2017).

The input data to Mapper is the (# time points)$\times$(# channels) dimensional matrix prepared by the preprocessing explained in Sec .

We choose the Euclidean metric as a similarity measure between the vectors in the time-space (i.e. column vectors) of the input matrix. The euclidean metric is suitable in this setting as the ranges and means of the data columns do not vary significantly Nielson et al. (2015). The choice of Euclidean metric is also proven to be successful in the previous applications of neuroimage data: In Romano et al. (2014), Mapper with Euclidean metric applied on sMRI data reveals high and low functioning neuro-phenotypes within Fragile X Syndrome. In Kyeong et al. (2017), the method on fMRI data identified two unique subgroups of ADHD using the Euclidean metric. In another fMRI study, a data-driven search for different metrics indicates that the Euclidean metric best localizes outcome measures Madan et al. (2017).

In the next step, the similarity information determined by the Euclidean metric is transformed into a low dimensional representation using a non-linear filter called t-SNE Hinton and Roweis (2002), which maintains the local geometry existing in the original time-space unlike more conventional linear filters such as PCA van der Maaten and Hinton (2008); Saggar et al. (2018). Multivariate and non-linear characteristics of inter-regional interactions suggest the use of non-linear methods such as t-SNE Reinen et al. (2018), DiCarlo et al. (2012).The data which is first reduced into two dimensions by t-SNE is then divided into overlapping bins. Following the earlier practice Lum et al. (2013), the time points in each bin are further clustered using single linkage clustering with the Euclidean metric, which is computationally more efficient compared to the other clustering methods, and which does not require an initial number of clusters.

The common practice in Mapper applications is to test a large grid of parameters (i.e. overlapping percentage and number of intervals) to find the most stable graphs. Even though the stability of the Mapper algorithm under various parameters was studied before under certain conditions Carrière and Oudot (2018); Kalyanaraman et al. (2017), we analyze several parameters of the algorithm to ensure the reliability of our result.

Centrality and Community Structure Analysis

The mathematical graphs obtained from Mapper can be investigated by focusing its structures on different scales. It is established through many applications that the intermediate (mesoscale) structures identify certain characteristics that the local scale analysis of nodes (or edges) and global level of summary statistics are unsuccessful to detect. In this paper, we concentrate on centrality and modularity mesoscale properties.

Centrality analysis of a network reveals the most important nodes (or edges) based on a quantification of node-node or node-edge relationships. The centrality of a node can be perceived as the communication ability with the other nodes or the closeness to the other nodes Estrada (2011). The centrality structure provides a perspective to comprehend how the brain states evolve during the ongoing task. The nodes with high centrality in the Mapper graph contain the most common brain activation patterns during the task. Here, we utilized four centrality measures: degree, eigenvalue, betweenness, and closeness. Based on the visual evidence from the box plots Fig. 2, Fig. 3, and Fig. 4 and the similar findings in Saggar et al. (2018), we claim for any one of those four centrality scores that

H_{WS} : *The mean of the centrality score of the nodes dominated by the working memory paradigm time points is greater than the mean of the centrality score of the nodes dominated by the story/math paradigm time points.*

H_{WM} : *The mean of the centrality score of the nodes dominated by the sensory-motor paradigm time points is greater than the mean of the centrality score of the nodes dominated by the working memory paradigm time points.*

H_{SM} : *The mean of the centrality score of the nodes dominated by the sensory-motor paradigm time points is greater than the mean of the centrality score of the nodes dominated by the story/math paradigm time points.*

Modularity is one of the most commonly used metric to detect and characterize the community structure of the networks. Detecting communities in brain networks, are useful to identify the sub-networks that correspond to specialized functional components Sporns and Betzel (2016). In this paper, we use modularity as defined in Newman (2006).

Analysis Pipeline

We summarize all the steps explained so far in the previous sections in Fig 5.

Earlier studies Saggar et al. (2018); Saggar and Uddin (2019); Duman et al. (2019) show that the topological properties of Mapper graphs are robust by construction to parameter perturbations. To ensure the reliability of the statistical results, we tested our null hypothesis using 48 different sets of Mapper parameters. The domains for # intervals, overlap %, and # clusters are $\{10,15,20\}$, $\{30,40,50,60\}$, and $\{5,10,15,20\}$, respectively. The parameter space is chosen in a way that the resulting Mapper graphs are connected to make modularity and centrality calculation possible. Statistically significant and reliable results are obtained for the large portion of parameter values (see Sec. for details).

To have a better understanding, we also track the steps of the proposed analysis with the story/math and sensory-motor paradigm time points of the subject 106521.

After concatenating the paradigms across the common channels, the subject 106521 is represented by a matrix of dimensions (357371×232). The first 177162 time points of the 357371 time points belong to the story/math paradigm and the rest to the motor-sensory. The Mapper algorithm with the projected data by SNE and the parameters 10, 50, and 10 corresponding to the number of intervals, percentage of overlap, and the number of clusters in the single linkage clustering, respectively, outputs the Mapper graph in Fig 6. It has 960 nodes and 13889 edges. The nodes are either in black if the majority of the time points in that node belong to the story/math paradigm or in green color if the majority of the time points in that node belong to the sensory-motor paradigm. In 70% of the nodes the story/math paradigm time

points are in majority and these nodes are on the periphery of the Mapper graph. The remaining 30% of the nodes are dominated by the sensory-motor paradigm time points which are placed mostly in the center of the graph.

Code Accessibility

The code described in the paper is available from the corresponding author upon reasonable request.

RESULTS

In this section, we discuss the results of the experiments whose details are explained in section . We check the reliability of our results by repeating the experiments with 48 different sets of Mapper parameters. The experiments are carried out in a Python environment using a workstation with 2 Nvidia GPUs (RTX 2080 Ti, 11 GB VRAM Per GPU), 10 Cores CPU (Intel i9-9820X), and 64 GB Memory.

Centrality of the Mapper Graphs

For every pairwise scenario, working memory vs. story/math, working memory vs. sensory-motor, and story/math vs. sensory-motor and for every subject, we calculate four different centrality scores, degree, eigenvector, betweenness, and closeness centralities of the nodes in the Mapper graphs. Moreover, to show that the results do not depend on the Mapper graph, we repeat the same experiment with 48 different sets of Mapper parameters. The Mapper parameter space is made of triples of the form (# intervals, overlap %, # clusters). The domains for # intervals, overlap %, and # clusters are $\{10,15,20\}$, $\{30,40,50,60\}$, and $\{5,10,15,20\}$, respectively.

We look at the pairwise results. In the working memory and story/math paradigms, there are 60 common subjects. Fig 2 shows that, regardless of the Mapper parameters, all four centrality scores clearly distinguish the nodes dominated by the working memory time points from the nodes dominated by the story/math time points. We want to confirm this visual difference through statistical tests. The most relevant statistical test to use is the paired t-test that compares the mean of the centrality scores of the nodes dominated by the working memory time-points (μ_W) and the mean of the centrality scores of the nodes dominated by the story/math paradigm's time-points (μ_S). However, the paired t-test only works under the assumption that sample points follow a normal distribution. Therefore, we shall check numerically using the Shapiro–Wilk normality test or visually using probability plots that the differences in centrality scores of different paradigms satisfy this fact.

There might be Mapper plots with the differences in the centrality scores not following a normal distribution. For example, the distribution of closeness centrality scores of the nodes of the Mapper graph with parameters 10-40-5 is non normal distribution with $p = 0.02$ Shapiro Wilk normality test (see Fig 7 for the probability plot). For such cases, we use the paired permutation test Good (2013) with the test statistic being the mean of the differences between the centrality scores. We shall clarify how the p value of the test statistics is calculated. First, we calculate the observed mean differences μ_{obs} between the working memory and the story/math paradigms. The permutation test assumes that there is no difference between the test statistics. The translation of this null hypothesis to our case is that there is no difference between the paradigms. Hence, we can create new data sets by swapping the centrality measures of the paradigms for the same subject. We compute the mean of the differences between the paradigms for every possible new data set and compare them to μ_{obs}. If the alternative hypothesis is that the means are not equal, then the p value is $2\min(p_l, p_g)$ where p_g (resp. p_l) is the probability of the mean of the differences being greater (resp. less) than μ_{obs}. If the alternative hypothesis is that one of the means is greater (resp. less) than the other mean, then the p is the probability of the mean of the differences being greater (resp. less) than μ_{obs}. As in the other hypothesis testing, if the p value is smaller than the significance level of 0.05, we say that the null hypothesis is not likely to be observed and favor the alternative. In Appendix, we illustrate the permutation test on the closeness centrality scores of the Mapper graph with parameters 10-40-5. In Table 1, we show how the paired permutation test creates a permuted data set. Later, the test statistics which is the mean of the differences in the centrality scores of the paradigms working memory and story/math are calculated. Going back to hypothesis testing, to verify our claims, we start with the null hypothesis:

H_0: *The mean of the centrality scores of the working memory nodes is equal to the mean of the centrality scores of the story/math nodes.*

Based on the Figs 2, 3, and 4, we expect H_0 to be rejected for all the Mapper parameters and for all centrality score types. Then, we verify which mean is greater by simply comparing the sample means. We look at the pairwise combinations one by one. To our expectations, in working memory and story/math combination, the p values in the columns $\mu_W = \mu_S$ of the Table 2 being less than 0.05 indicate that we shall reject the null hypothesis in favor of its alternative which is that μ_W and μ_S are significantly different. Moreover, as $\mu_S < \mu_W$ and halves of all the p values in Table 2 are also less than 0.05, we can deduce that the mean of the centrality scores of the working memory nodes μ_W is significantly greater than the mean of the centrality scores of the story/math nodes μ_S.

In the case of story/math and sensory-motor combination with 43 common subjects, by going through similar steps as above, we come to the conclusion using the test results in Table 3, that the mean of the centrality scores of the sensory-motor nodes μ_M is significantly greater than the mean of the centrality scores of the story/math nodes μ_S.

For the final combination of working memory and sensory-motor with 21 common subjects, the table 4 shows that the p values of either the paired t-test or the permutation test under the null hypothesis are all greater than the significance level of 0.05 indicating that there is not enough evidence to reject the null hypothesis. Hence, we conclude for all types of centrality scores that mean the mean of the centrality scores of the working memory μ_W and sensory-motor μ_M are not significantly different.

The above discussions show that, when compared pairwise, the centrality score of the nodes dominated by the time points of the story/math paradigm is the smallest. We summarize our findings in the Table 5.

Community Structure and Response Time

Subjects' performances during the working memory and story/math experimental paradigms are scored and timed. In this section, we investigate if the modularity structure of the Mapper graphs is related to these measurements.

The distribution of modularity scores of all subjects are shown by box plots for different set of mapper parameters in Fig 8. x-axis of the figure represents different set of mapper parameter. The interval parameter given by the first two numbers are either 10, 15 or 20. The following two numbers for the cluster parameter are either 30, 40, 50 or 60. The remaining numbers represents the overlap percentage which is either 5, 10, 15 or 20. Once we give a closer look at Fig 8, we observe that the median of the modularity scores tends to

1. increase with the increase in the interval parameter as an increase in that parameter results in more nodes, hence more edges in the Mapper graph (see Fig 9),

2. decrease with the increase in cluster parameter as an increase in that parameter results in a decrease in the number of edges (see Fig 10),

3. non-decrease with the increase in the overlap percentage parameter as an increase in that parameter up to certain level results in a high number of edges and beyond that level less number of edges since some of the small nodes is absorbed by the larger ones. According to Fig 11, that level is between 50% and 60% for our data set.

Moreover, the experiment results show that the modularity score of the Mapper graphs is negatively correlated to the reaction time. According to Table 6, the negative correlation is observed in all the Mapper graphs with different parameters. All correlation scores, with the strongest recorded at the parameters $(10-40-5)$ (see Fig 12), are weak and non-significant.

We also note that the strongest correlation scores are associated with the lowest clustering parameters as an increase in this parameter decreases the number of edges within the same interval which more likely contains similar tasks. (see Fig 13)

Other Methods

We also visualize the time points before the Mapper algorithm. In Fig 14, we see that the story/math paradigm time points overlap with the sensory-motor paradigm time points which indicates that a distance-based clustering would not distinguish them.

DISCUSSION

The neural oscillations in the brain change rapidly in response to sensory and cognitive stimulations Pfurtscheller and Lopes da Silva (1999). As this fact implies the quick change in functional connectivity patterns, it is crucial to analyze dynamic connectivity to gain insight into how the information is processed in the brain. There is also increasing clinical interest in dynamic functional connectivity, which is shown to be perturbed by diseases such as schizophrenia Damaraju et al. (2014), bipolar disorder Rashid et al. (2014), and depression Demirtaş et al. (2016). For clinical applications, there is a need to have methods that derive a meaningful conclusion from high spatiotemporal dimensional data on the individual level. Moreover, state-of-the-art methods require the temporal and spatial collapse of the data, which may result in information loss. Saggar et al. Saggar et al. (2018) has recently addressed these issues for fMRI data using the Mapper algorithm that provides an interactive simple visualization of the brain dynamics on an individual level during ongoing cognitive tasks. However, it is hard to detect the rapid changes in neural activity using hemodynamic signals from fMRI, as they are the proxy of neural activity. In this current work, we extend this topological approach to high temporal resolution MEG data which can measure the fast fluctuations directly avoiding the autocorrelation structure caused by the hemodynamic response in fMRI.

This new topological approach to the MEG data provides an interactive mathematical graph that tracks the brain configuration patterns of each participant during the sensory-motor, story/math, and working memory tasks. The Mapper graph for each participant is obtained from pairwise concatenation of the MEG data sets of different tasks which are not temporally and spatially[1] collapsed in prior. The mesoscale graph invariants (i.e. centrality and modularity) of the resulting graphs uncover temporal characteristics of the brain configuration.In line with fMRI results Saggar et al. (2018) the centrality invariants statistically differentiate story/math and working memory tasks . Working memory task being cognitively more demanding has greater centrality values than the story/math data set on the individual level. This result is in accordance with the earlier neurophysiological findings of brain dynamics Liu and Duyn (2013); Ponce-Alvarez et al. (2015) and previous fMRI results Saggar et al. (2018) where the higher similarity between brain regions is observed if the task requires stronger cognitive involvement.

As noted by O'Neill O'Neill et al. (2018), there are two existing groups of approaches for aggregating the time points to measure connectivity between brain regions: (i) using multiple successive time points such as in the case of sliding windows[2], and (ii) aggregating across the same time point of multiple trials to generate connectivity dynamics. The first type of approach is mainly used for experiments without any trials (e.g. resting state), while the latter requires multiple task trials. The Mapper graph addresses the limitation of both approaches and can be used in the experiments both with or without trials. While there are parameters in the Mapper algorithm, the graphs are shown to be robust to the parameter choice. This is not the case with the sliding windows (or similar) methods, as the results with small window width are governed by the noise, while too large windows are not sensitive to rapid fluctuations. Unlike sliding windows, the temporal resolution is also preserved during the calculation of Mapper graphs. Moreover, the information loss caused by averaging over trials is avoided in the proposed Mapper pipeline.

Mapper algorithm applied on high temporal resolution raw MEG data ($\sim$ 800,000 time points) also contributes to biological understanding. The following possible connectomic biomarker can be extracted from the Mapper graph: The centrality of the Mapper graph that distinguishes working memory, story/math, and sensory-motor tasks.

The Mapper graphs with high modularity (i.e. the nodes containing similar tasks have dense connections between them but sparse connections with the remaining nodes) have negative and non-significant correlation with the response time of the cognitive tasks. A stronger but statistically weak correlation between modularity and response time is also found in fMRI studies Saggar et al. (2018). The weaker correlation in MEG is due to a high number of time points ($\sim$800,000) with higher noise compared to fMRI data, which has about 1000 time points. In order to improve this results, the future studies can investigate different filter functions other than t-SNE. Unlike fMRI, the proposed approach on MEG does not detect any correlation between accuracy and modularity possibly due to the high level of noise.

[1]While the filter function t-SNE maps the time points to two dimensional space to make the visualization possible, it is still possible to trace back the activated locations in the brain from the nodes of the mapper graph Saggar et al. (2018). Hence, the spatial information is not lost during the process.

[2]Note that sliding windows method calculates region-by-region connectivity on each time window and then explores the change in standard FC patterns during the experiment.

Another mesoscale structure that provides biological understanding is centrality. The four centrality invariants used in our analysis give similar outcomes for each participant's Mapper graphs. The high number of time points ($\sim$400,000) per paradigm and the computational limitations necessitate the pairwise comparison of the working memory, story/math, and sensory-motor paradigms. The centrality of working memory and the sensory-motor tasks are shown to be greater than the story/math tasks due to higher cognitive demand, as a similar but statistically less significant result is also observed in fMRI Saggar et al. (2018). This supports earlier findings indicating that the subjects performing tasks with higher cognitive efforts have higher similarity in whole-brain activation patterns compared to the periods of rest Liu and Duyn (2013); Ponce-Alvarez et al. (2015). Thus, the nodes containing time points of cognitively demanding tasks have more edges connecting resulting in higher centrality scores than the nodes of less demanding tasks. In addition, no difference between the centrality of sensory-motor tasks and the centrality of working memory is observed. This result, which contradicts the fMRI results for the same tasks in Saggar et al. (2018), can be explained by the low number of common subjects ($n = 21$) who performed both tasks. While a little fluctuation in the connectedness of specific brain areas during the motor-related tasks that were previously reported supports our findings Bassett et al. (2013), the neurophysiological relationship between the motor and the cognitive skills is more complex and still under discussion. The proposed topological approach might shed light on this issue from the perspective of overall brain dynamics.

One of the limitations in this current study is the computational expense of generating a Mapper graph from 350,000-400,000 time points of the MEG recordings from each individual. It is worth noting that new software packages such as NeuMapper Geniesse et al. (2022) are reported to be much more efficient compared to KeplerMapper which is used in the current study. Another limitation is to determine the minimum number of time points that are required to produce a robust generation of Mapper graphs and corresponding graph invariants. As it might not be feasible to acquire sufficiently long recordings from individuals for clinical studies. The other possible criticism might be the low number of subjects ($n = 21$) in the concatenated sensory-motor and working memory data which potentially results in higher adjusted p-values. The other pairs working memory vs. story/math ($n = 60$) and sensory-motor vs. story/math ($n = 45$) have a higher number of subjects where the results are more statistically significant. Even though it is shown that the results are robust to parameter variation, it will be useful to find a parameter and filter function selection and exploration framework for MEG data. In Geniesse et al. (2022), the authors propose an algorithm that leverages the autocorrelation structure present in fMRI data due to the slow hemodynamic response, which is not the case in MEG data. Another consideration is that results will be mainly driven by the alpha band, while different dynamics might occur in the other bands. Future work is required to do the same analysis after filtering data in various bands.

The ultimate aim of this research is to extract novel biomarkers to be used in translational studies given high temporal dimensional, minimally processed MEG (or EEG) data sets of individuals. For example, brain networks extracted from EEG of ADHD group have a significantly lower clustering coefficient and longer characteristic path length than the ones of the control group Jang et al. (2020). Hence, Mapper graphs of the individuals with ADHD traits are expected to have lower centrality measures than normal individuals. On the other hand, it is argued by Saggar and colleagues in Saggar et al. (2018) that higher centrality results are anticipated from the data of depressed patients compared to healthy individuals, as depressed patients show more functional connectivity than their healthy counterparts using seed-based connectivity approach Berman et al. (2011).

CONCLUSIONS

Using the graph theoretical invariants of Mapper graphs, we found that the centrality scores of the working memory task are significantly higher than the centrality scores of the story/math task; and the centrality scores of the sensory-motor task are significantly higher than the centrality scores of the story/math task. These results suggest that whole-brain activation patterns are more similar for tasks requiring higher cognitive effort when compared to periods of rest. Likewise, it is demonstrated that there is a weak negative and non-significant correlation between the community structure of the graph and the response time for the working memory and story/math tasks. Although the high number of time points and associated noise contributed to the weak correlation and its non-significance in MEG, this result along with the similar fMRI result has a potential to be improved as the individuals with a specific whole-brain organization are expected to have faster reaction times. The present study shows the potential contribution

of the topological data analysis method (i.e. Mapper) to translational studies, while the resulting interactive graphs reveal brain reconfiguration of different frequencies in noisy high-temporal-resolution MEG data at an individual level without losing any information by spatiotemporal collapsing.

As a future direction, it will be interesting to investigate how sensitive the Mapper algorithm is to spatiotemporal collapsing and preprocessing steps of MEG data. Specifically, it is essential to compare concatenated MEG data with continuous MEG data using the Mapper approach, even though they earlier revealed similar qualitative and quantitative results during rest and task Fair et al. (2007), Gavrilescu et al. (2008), Cheng et al. (2015), Zhu et al. (2017).

Another concern in the current study is applying Mapper on channel-level MEG data recorded by magnetometers; as different source configuration can produce similar MEG channel-level maps, while similar source level data can produce different channel-level signals due different head positions. To address this issue, future studies should investigate application of Mapper on a set of nodes in the source space.

Another direction is to apply Mapper to a set of nodes in the source space rather than to channel-level MEG data recorded by magnetometers. This will address the concern about the fact that different source configuration can produce similar MEG channel-level maps, while different head positions could produce different channel-level patterns from similar source level patterns.

In this study, we have chosen Euclidean distance as a similarity measure and t-SNE as a Mapper filter function. Inspired by manifold learning Tenenbaum et al. (2000), the use geodesic distances in Mapper algorithm has been recently suggested as the geodesic distances preserve the locality of the original high dimensional data better than Euclidean distance after dimension reduction Saggar et al. (2022a), Saggar et al. (2022b). Moreover, the filter function t-SNE can produce artificial clusters in low dimensions. Hence, exploring different similarity measures and filter functions in a future study can provide different insights from the MEG data.

One should also investigate the relationship between mapper graphs and MEG/EEG microstates in cognitive tasks. It is expected that the limited number of microstates are highly connected in mapper graphs due to their similar topography.

ACKNOWLEDGMENT

The authors acknowledge the referees for their insightful comments. The authors would also like to express their appreciation to Linda Geerligs for the valuable discussions during the planning and development of this paper. Part of this research was conducted during a visit of AET to Donders Institute, Netherlands.

	Observed		Permuted	
Subjects	Wrkmem	Storym	Wrkmem	Storym
100307	0.2563	0.2006	0.2563	0.2006
102816	0.2372	0.1864	0.2372	0.1864
104012	0.2388	0.2045	0.2388	0.2045
106521	0.2301	0.1881	0.2301	0.1881
108323	0.2477	0.175	0.2477	0.175
109123	0.259	0.1862	0.259	0.1862
116726	0.2235	0.1968	0.2235	0.1968
133019	0.2497	0.1992	0.2497	0.1992
140117	0.2349	0.1942	0.2349	0.1942
146129	0.251	0.1871	0.251	0.1871
149741	0.2653	0.1967	0.2653	0.1967
151526	0.2534	0.1843	0.2534	0.1843
156334	0.2549	0.1963	0.2549	0.1963
158136	0.2528	0.1914	0.2528	0.1914
162026	0.2557	0.1981	0.2557	0.1981
166438	0.2579	0.2036	0.2579	0.2036
169040	0.2604	0.1883	**0.1883**	**0.2604**
175540	0.2364	0.1889	0.2364	0.1889
182840	0.2549	0.187	0.2549	0.187
185442	0.238	0.1748	0.238	0.1748
191033	0.2458	0.2021	0.2458	0.2021
191437	0.2373	0.1814	0.2373	0.1814
192641	0.2477	0.1749	0.2477	0.1749
195041	0.2562	0.1878	0.2562	0.1878
200109	0.2378	0.2118	0.2378	0.2118
204521	0.2449	0.1794	0.2449	0.1794
205119	0.2504	0.197	0.2504	0.197
212318	0.2413	0.1867	0.2413	0.1867
212823	0.2454	0.2006	0.2454	0.2006
214524	0.2452	0.2049	0.2452	0.2049
223929	0.2289	0.2115	0.2289	0.2115
248339	0.2403	0.1728	0.2403	0.1728
255639	0.246	0.1714	0.246	0.1714
257845	0.2565	0.2003	**0.2003**	**0.2565**
283543	0.2675	0.201	0.2675	0.201
293748	0.2587	0.1883	0.2587	0.1883
353740	0.2471	0.1941	0.2471	0.1941
433839	0.2485	0.1766	0.2485	0.1766
512835	0.2546	0.1846	0.2546	0.1846
555348	0.2528	0.1824	0.2528	0.1824
568963	0.2376	0.1933	**0.1933**	**0.2376**
599671	0.2382	0.1812	0.2382	0.1812
601127	0.2503	0.1965	0.2503	0.1965
660951	0.2488	0.2012	0.2488	0.2012
662551	0.2379	0.1976	0.2379	0.1976
665254	0.2509	0.1817	0.2509	0.1817
667056	0.2392	0.1856	0.2392	0.1856
679770	0.2308	0.1993	0.2308	0.1993
706040	0.2086	0.1677	0.2086	0.1677
707749	0.2122	0.166	0.2122	0.166
715950	0.2473	0.1914	0.2473	0.1914
725751	0.2648	0.1928	0.2648	0.1928
735148	0.2398	0.2021	0.2398	0.2021
783462	0.2479	0.1897	0.2479	0.1897
814649	0.2379	0.1899	0.2379	0.1899
825048	0.2393	0.1993	0.2393	0.1993
872764	0.2388	0.1849	0.2388	0.1849
877168	0.2377	0.1856	0.2377	0.1856
891667	0.2473	0.1943	0.2473	0.1943
917255	0.2564	0.2027	0.2564	0.2027

Table 1. Permutation Test. Bold rows represent the swapped centrality scores to create a permutation of the observed closeness centrality scores of the Mapper graph with parameters 10-40-5. The permutation test compares the mean of the differences (Wrkmem - Storym) of the permuted centrality scores to the mean of the differences of the observed centrality scores which are 0.0490 and 0.0547, respectively.

REFERENCES

Allen, E. A., Damaraju, E., Plis, S. M., Erhardt, E. B., Eichele, T., and Calhoun, V. D. (2012). Tracking whole-brain connectivity dynamics in the resting state. *Cerebral Cortex*, 24(3):663–676.

Andjelković, M., Tadić, B., and Melnik, R. (2020). The topology of higher-order complexes associated with brain hubs in human connectomes. *Scientific Reports*, 10(1):17320.

Antonakakis, M., Dimitriadis, S. I., Zervakis, M., Papanicolaou, A. C., and Zouridakis, G. (2020). Aberrant whole-brain transitions and dynamics of spontaneous network microstates in mild traumatic brain injury. *Frontiers in Computational Neuroscience*, 13.

Armeni, K., Güçlü, U., van Gerven, M., and Schoffelen, J.-M. (2022). A 10-hour within-participant magnetoencephalography narrative dataset to test models of language comprehension. *Scientific Data*, 9(1):278.

Baker, A. P., Brookes, M. J., Rezek, I. A., Smith, S. M., Behrens, T., Probert Smith, P. J., Woolrich, M., and Culham, J. C. (2014). Fast transient networks in spontaneous human brain activity. *eLife*, 3:e01867.

Barch, D. M., Burgess, G. C., Harms, M. P., Petersen, S. E., Schlaggar, B. L., Corbetta, M., Glasser, M. F., Curtiss, S., Dixit, S., Feldt, C., Nolan, D., Bryant, E., Hartley, T., Footer, O., Bjork, J. M., Poldrack, R., Smith, S., Johansen-Berg, H., Snyder, A. Z., and Van Essen, D. C. (2013). Function in the human

Parameter	Degree Centrality		Eigenvector Centrality		Betweenness Centrality		Closeness Centrality	
(I-O-C)	$\mu_W = \mu_S$	Test Type	$\mu_W = \mu_S$	Test Type	$\mu_W = \mu_S$	Test Type	$\mu_W = \mu_S$	Test Type
10305	**0.009**	(P)	1.34E-39	(T)	4.23E-42	(T)	1.49E-36	(T)
10405	3.87E-33	(T)	8.91E-38	(T)	2.64E-37	(T)	**0.009**	(P)
10505	8.37E-34	(T)	1.22E-37	(T)	1.68E-38	(T)	1.64E-38	(T)
15305	4.28E-34	(T)	3.40E-43	(T)	4.07E-41	(T)	2.08E-31	(T)
15405	3.27E-33	(T)	1.84E-42	(T)	1.43E-40	(T)	4.68E-35	(T)
15505	9.31E-33	(T)	3.26E-41	(T)	1.20E-39	(T)	2.11E-37	(T)
15605	1.52E-35	(T)	9.00E-39	(T)	1.85E-41	(T)	3.24E-38	(T)
20305	1.30E-34	(T)	3.70E-45	(T)	8.55E-41	(T)	7.20E-29	(T)
20405	3.54E-33	(T)	5.49E-45	(T)	2.00E-42	(T)	2.09E-31	(T)
20505	1.58E-31	(T)	1.51E-43	(T)	4.77E-41	(T)	1.31E-34	(T)
20605	6.88E-35	(T)	1.30E-41	(T)	3.94E-42	(T)	7.34E-38	(T)
103010	2.14E-38	(T)	2.71E-42	(T)	5.13E-45	(T)	1.40E-32	(T)
104010	2.96E-35	(T)	2.31E-39	(T)	5.54E-40	(T)	1.18E-33	(T)
105010	1.32E-35	(T)	8.55E-39	(T)	1.30E-39	(T)	4.40E-36	(T)
106010	5.00E-39	(T)	**2.56E-36**	(T)	1.58E-42	(T)	1.66E-38	(T)
153010	3.02E-36	(T)	3.18E-45	(T)	1.49E-38	(T)	1.56E-28	(T)
154010	9.81E-36	(T)	2.94E-44	(T)	2.29E-41	(T)	3.03E-29	(T)
155010	1.15E-35	(T)	6.53E-44	(T)	1.80E-42	(T)	2.46E-33	(T)
156010	6.66E-37	(T)	1.85E-40	(T)	1.31E-42	(T)	7.83E-36	(T)
203010	2.93E-35	(T)	3.81E-46	(T)	**0.009**	(P)	8.87E-27	(T)
204010	3.28E-35	(T)	4.43E-46	(T)	**0.009**	(P)	2.32E-27	(T)
205010	1.10E-34	(T)	9.81E-46	(T)	**0.009**	(P)	4.72E-30	(T)
206010	1.32E-36	(T)	4.41E-44	(T)	1.43E-44	(T)	1.58E-33	(T)
103015	6.66E-39	(T)	5.22E-44	(T)	2.30E-43	(T)	3.70E-31	(T)
104015	1.89E-36	(T)	5.35E-41	(T)	1.51E-42	(T)	5.81E-31	(T)
105015	1.53E-36	(T)	1.20E-39	(T)	2.62E-39	(T)	3.43E-34	(T)
153015	2.78E-36	(T)	1.24E-45	(T)	3.01E-37	(T)	6.75E-28	(T)
154015	3.49E-36	(T)	3.40E-45	(T)	3.87E-39	(T)	2.25E-27	(T)
155015	1.43E-36	(T)	5.58E-45	(T)	1.36E-43	(T)	2.61E-31	(T)
156015	2.11E-37	(T)	1.19E-41	(T)	1.34E-43	(T)	5.85E-34	(T)
203015	4.21E-35	(T)	3.94E-46	(T)	7.42E-34	(T)	2.08E-26	(T)
204015	2.44E-35	(T)	2.77E-46	(T)	2.21E-36	(T)	7.02E-26	(T)
205015	3.76E-35	(T)	4.16E-46	(T)	6.88E-40	(T)	2.78E-27	(T)
206015	4.64E-37	(T)	4.29E-45	(T)	1.16E-44	(T)	6.35E-31	(T)
103020	9.99E-39	(T)	1.40E-44	(T)	2.61E-42	(T)	1.40E-44	(T)
104020	8.23E-37	(T)	7.69E-42	(T)	8.51E-42	(T)	7.69E-42	(T)
105020	2.20E-37	(T)	5.58E-41	(T)	3.94E-41	(T)	5.58E-41	(T)
153020	1.00E-35	(T)	1.39E-45	(T)	3.68E-35	(T)	1.39E-45	(T)
154020	4.86E-36	(T)	1.69E-45	(T)	4.59E-38	(T)	1.69E-45	(T)
155020	1.06E-36	(T)	4.68E-45	(T)	2.05E-42	(T)	4.68E-45	(T)
156020	8.73E-38	(T)	1.25E-42	(T)	8.42E-44	(T)	1.25E-42	(T)
203020	1.09E-34	(T)	1.09E-45	(T)	5.00E-32	(T)	1.09E-45	(T)
204020	5.80E-35	(T)	9.05E-46	(T)	1.17E-34	(T)	9.05E-46	(T)
205020	4.99E-35	(T)	4.64E-46	(T)	4.20E-38	(T)	4.64E-46	(T)
206020	4.43E-37	(T)	1.16E-45	(T)	3.16E-44	(T)	1.16E-45	(T)

Table 2. Working memory vs. Story/math. Bonferroni corrected p values of either the paired t-test or the paired permutation test for all types of centrality scores. Highlighted p values in every column represent the maximum of that column. Note that maximum values in all columns are less than the significance level of 0.05 and so are their halves.

connectome: Task-fmri and individual differences in behavior. *NeuroImage*, 80:169–189.

Bassett, D. S., Wymbs, N. F., Porter, M. A., Mucha, P. J., Carlson, J. M., and Grafton, S. T. (2011). Dynamic reconfiguration of human brain networks during learning. *Proceedings of the National Academy of Sciences*, 108(18):7641–7646.

Bassett, D. S., Wymbs, N. F., Rombach, M. P., Porter, M. A., Mucha, P. J., and Grafton, S. T. (2013). Task-based core-periphery organization of human brain dynamics. *PLOS Computational Biology*, 9(9):e1003171–.

Bastos, A. M. and Schoffelen, J.-M. (2016). A tutorial review of functional connectivity analysis methods and their interpretational pitfalls. *Frontiers in Systems Neuroscience*, 9:175.

Berman, M. G., Peltier, S., Nee, D. E., Kross, E., Deldin, P. J., and Jonides, J. (2011). Depression, rumination and the default network. *Soc Cogn Affect Neurosci*, 6(5):548–555.

Billings, J., Saggar, M., Hlinka, J., Keilholz, S., and Petri, G. (2021). Simplicial and topological descriptions of human brain dynamics. *Network Neuroscience*, 5(2):549–568.

Binder, J. R., Gross, W. L., Allendorfer, J. B., Bonilha, L., Chapin, J., Edwards, J. C., Grabowski, T. J., Langfitt, J. T., Loring, D. W., Lowe, M. J., Koenig, K., Morgan, P. S., Ojemann, J. G., Rorden, C., Szaflarski, J. P., Tivarus, M. E., and Weaver, K. E. (2011). Mapping anterior temporal lobe language areas with fmri: A multicenter normative study. *NeuroImage*, 54(2):1465–1475.

Bray, S., Chang, C., and Hoeft, F. (2009). Applications of multivariate pattern classification analyses in developmental neuroimaging of healthy and clinical populations. *Frontiers in Human Neuroscience*, 3:32.

Breakspear, M. (2002). Nonlinear phase desynchronization in human electroencephalographic data. *Human Brain Mapping*, 15(3):175–198.

Brookes, M. J., Tewarie, P. K., Hunt, B. A. E., Robson, S. E., Gascoyne, L. E., Liddle, E. B., Liddle, P. F., and Morris, P. G. (2016). A multi-layer network approach to meg connectivity analysis. *NeuroImage*,

Parameter	Degree Centrality		Eigenvector Centrality		Betweenness Centrality		Closeness Centrality	
(I-O-C)	$\mu_S = \mu_M$	Test Type	$\mu_S = \mu_M$	Test Type	$\mu_S = \mu_M$	Test Type	$\mu_S = \mu_M$	Test Type
10305	**0.009**	(P)	1.78E-31	(T)	**0.009**	(P)	**0.009**	(P)
10405	**0.009**	(P)	4.91E-31	(T)	**0.009**	(P)	**0.009**	(P)
10505	**0.009**	(P)	3.58E-29	(T)	**0.009**	(P)	**0.009**	(P)
15305	**0.009**	(P)	1.84E-34	(T)	**0.009**	(P)	**0.009**	(P)
15405	**0.009**	(P)	2.47E-33	(T)	**0.009**	(P)	**0.009**	(P)
15505	**0.009**	(P)	**0.009**	(P)	**0.009**	(P)	**0.009**	(P)
15605	**0.009**	(P)	**0.009**	(P)	**0.009**	(P)	**0.009**	(P)
20305	**0.009**	(P)	2.35E-35	(T)	**0.009**	(P)	**0.009**	(P)
20405	**0.009**	(P)	**0.009**	(P)	**0.009**	(P)	**0.009**	(P)
20505	**0.009**	(P)	**0.009**	(P)	**0.009**	(P)	**0.009**	(P)
20605	**0.009**	(P)	9.49E-33	(T)	**0.009**	(P)	**0.009**	(P)
103010	**0.009**	(P)	1.12E-32	(T)	**0.009**	(P)	**0.009**	(P)
104010	**0.009**	(P)	8.19E-32	(T)	**0.009**	(P)	**0.009**	(P)
105010	**0.009**	(P)	1.62E-30	(T)	**0.009**	(P)	**0.009**	(P)
153010	**0.009**	(P)	8.73E-35	(T)	**0.009**	(P)	**0.009**	(P)
154010	**0.009**	(P)	8.37E-35	(T)	**0.009**	(P)	**0.009**	(P)
155010	**0.009**	(P)	1.24E-33	(T)	**0.009**	(P)	**0.009**	(P)
156010	**0.009**	(P)	2.83E-31	(T)	**0.009**	(P)	**0.009**	(P)
203010	3.87E-30	(T)	9.59E-35	(T)	3.8E-30	(T)	**0.009**	(P)
204010	**0.009**	(P)	5.49E-35	(T)	**0.009**	(P)	**0.009**	(P)
205010	**0.009**	(P)	6.84E-35	(T)	**0.009**	(P)	**0.009**	(P)
206010	**0.009**	(P)	**0.009**	(P)	**0.009**	(P)	**0.009**	(P)
103015	**0.009**	(P)	6.43E-33	(T)	**0.009**	(P)	**0.009**	(P)
104015	**0.009**	(P)	1.23E-32	(T)	**0.009**	(P)	**0.009**	(P)
105015	**0.009**	(P)	1.27E-30	(T)	**0.009**	(P)	**0.009**	(P)
153015	6.66E-30	(T)	1.11E-34	(T)	**0.009**	(P)	**0.009**	(P)
154015	**0.009**	(P)	1.04E-34	(T)	**0.009**	(P)	**0.009**	(P)
155015	**0.009**	(P)	**0.009**	(P)	**0.009**	(P)	**0.009**	(P)
156015	**0.009**	(P)	5.04E-32	(T)	9.72E-32	(T)	**0.009**	(P)
203015	8.1E-29	(T)	1.36E-33	(T)	**0.009**	(P)	**0.009**	(P)
204015	2.13E-29	(T)	8.14E-35	(T)	1.96E-30	(T)	**0.009**	(P)
205015	**0.009**	(P)	1.62E-34	(T)	**0.009**	(P)	**0.009**	(P)
206015	**0.009**	(P)	**0.009**	(P)	**0.009**	(P)	**0.009**	(P)
103020	2.62E-29	(T)	6.21E-33	(T)	**0.009**	(P)	**0.009**	(P)
104020	**0.009**	(P)	1.21E-32	(T)	**0.009**	(P)	**0.009**	(P)
105020	**0.009**	(P)	4.91E-31	(T)	1.55E-30	(T)	**0.009**	(P)
106020	**0.009**	(P)	1.68E-28	(T)	5.04E-28	(T)	**0.009**	(P)
153020	5.49E-29	(T)	2.43E-34	(T)	**0.009**	(P)	**0.009**	(P)
154020	1.23E-29	(T)	3.19E-34	(T)	**0.009**	(P)	**0.009**	(P)
155020	**0.009**	(P)	**0.009**	(P)	**0.009**	(P)	**0.009**	(P)
156020	**0.009**	(P)	**0.009**	(P)	1.44E-31	(T)	**0.009**	(P)
203020	6.39E-28	(T)	6.61E-33	(T)	**0.009**	(P)	**0.009**	(P)
204020	1.69E-28	(T)	8.91E-34	(T)	6.7E-29	(T)	**0.009**	(P)
205020	1.75E-29	(T)	6.03E-34	(T)	**0.009**	(P)	**0.009**	(P)
206020	**0.009**	(P)	**0.009**	(P)	**0.009**	(P)	**0.009**	(P)

Table 3. Story/math vs. Sensory-motor. Bonferroni corrected p values of either the paired t-test or the paired permutation test for all types of centrality scores. Highlighted p values in every column represent the minimum of that column. Note that the minimum values in all columns are less than the significance level of 0.05 and so are their halves.

132:425–438.

Brovelli, A., Badier, J.-M., Bonini, F., Bartolomei, F., Coulon, O., and Auzias, G. (2017). Dynamic reconfiguration of visuomotor-related functional connectivity networks. *Journal of Neuroscience*, 37(4):839–853.

Carbo, E. W. S., Hillebrand, A., van Dellen, E., Tewarie, P., de Witt Hamer, P. C., Baayen, J. C., Klein, M., Geurts, J. J. G., Reijneveld, J. C., Stam, C. J., and Douw, L. (2017). Dynamic hub load predicts cognitive decline after resective neurosurgery. *Scientific Reports*, 7:42117 EP –.

Carlsson, G. (2014). Topological pattern recognition for point cloud data. *Acta Numerica*, 23:289–368.

Carrière, M. and Oudot, S. (2018). Structure and stability of the one-dimensional mapper. *Foundations of Computational Mathematics*, 18(6):1333–1396.

Centeno, E. G. Z., Moreni, G., Vriend, C., Douw, L., and Santos, F. A. N. (2022). A hands-on tutorial on network and topological neuroscience. *Brain Structure and Function*, 227(3):741–762.

Chan, J. M., Carlsson, G., and Rabadan, R. (2013). Topology of viral evolution. *Proceedings of the National Academy of Sciences*, 110(46):18566–18571.

Chang, C. and Glover, G. H. (2010). Time–frequency dynamics of resting-state brain connectivity measured with fmri. *NeuroImage*, 50(1):81 – 98.

Cheng, L., Wu, Z., Sun, J., Fu, Y., Wang, X., Yang, G.-Y., Miao, F., and Tong, S. (2015). Reorganization of motor execution networks during sub-acute phase after stroke. *IEEE Trans Neural Syst Rehabil Eng*, 23(4):713–723.

Chiniforooshan Esfahani, I. (2023). A data-driven physics-informed neural network for predicting the viscosity of nanofluids. *AIP Advances*, 13(2):025206.

Damaraju, E., Allen, E. A., Belger, A., Ford, J. M., McEwen, S., Mathalon, D. H., Mueller, B. A., Pearlson, G. D., Potkin, S. G., Preda, A., Turner, J. A., Vaidya, J. G., van Erp, T. G., and Calhoun, V. D. (2014). Dynamic functional connectivity analysis reveals transient states of dysconnectivity in

Parameter	Degree Centrality		Eigenvector Centrality		Betweenness Centrality		Closeness Centrality	
(I-O-C)	$\mu_M = \mu_W$	Test Type	$\mu_M = \mu_W$	Test Type	$\mu_M = \mu_W$	Test Type	$\mu_M = \mu_W$	Test Type
10305	0.184	(T)	0.164	(T)	0.203	(T)	0.522	(T)
10405	0.198	(T)	0.167	(T)	0.204	(T)	0.396	(T)
10505	0.262	(T)	0.173	(T)	0.227	(T)	0.498	(T)
15305	0.126	(T)	0.134	(T)	0.165	(T)	0.248	(T)
15405	0.137	(T)	0.11	(T)	0.182	(T)	0.215	(T)
15505	0.165	(T)	0.167	(T)	0.174	(T)	0.288	(T)
15605	0.175	(T)	0.157	(T)	0.19	(T)	0.254	(T)
20305	0.0973	(T)	0.169	(T)	0.175	(T)	0.261	(T)
20405	**0.0775**	(T)	0.132	(T)	0.139	(T)	0.256	(T)
20505	0.0992	(T)	0.128	(T)	0.185	(T)	0.24	(T)
20605	0.156	(T)	0.129	(T)	0.202	(T)	0.34	(T)
103010	0.257	(T)	0.246	(T)	0.578	(T)	0.771	(T)
104010	0.231	(T)	0.227	(T)	0.447	(T)	0.686	(T)
105010	0.217	(T)	0.198	(T)	0.235	(T)	0.317	(T)
106010	0.387	(T)	0.305	(T)	0.869	(T)	0.611	(T)
153010	0.121	(T)	0.131	(T)	0.263	(T)	0.192	(T)
154010	0.126	(T)	**0.106**	(T)	0.177	(T)	0.331	(T)
155010	0.149	(T)	0.186	(T)	0.189	(T)	0.351	(T)
156010	0.167	(T)	0.163	(T)	0.282	(T)	0.235	(T)
203010	0.0884	(T)	0.122	(T)	0.136	(T)	0.147	(T)
204010	0.0921	(T)	0.12	(T)	0.159	(T)	0.227	(T)
205010	0.103	(T)	0.115	(T)	0.186	(T)	0.272	(T)
206010	0.131	(T)	0.137	(T)	0.188	(T)	0.261	(T)
103015	0.202	(T)	0.213	(T)	0.297	(T)	0.559	(T)
104015	0.205	(T)	0.188	(T)	0.408	(T)	0.578	(T)
105015	0.203	(T)	0.19	(T)	0.296	(T)	0.443	(T)
106015	0.335	(T)	0.298	(T)	0.667	(T)	0.606	(T)
153015	0.104	(T)	0.107	(T)	0.139	(T)	**0.124**	(T)
154015	0.112	(T)	0.117	(T)	0.153	(T)	0.307	(T)
155015	0.118	(T)	0.133	(T)	0.153	(T)	0.387	(T)
156015	0.131	(T)	0.148	(T)	0.136	(T)	0.331	(T)
203015	0.0893	(T)	0.14	(T)	0.101	(T)	0.13	(T)
204015	0.0926	(T)	0.138	(T)	0.112	(T)	0.165	(T)
205015	0.108	(T)	0.131	(T)	0.172	(T)	0.247	(T)
206015	0.124	(T)	0.13	(T)	0.122	(T)	0.232	(T)
103020	0.257	(T)	0.25	(T)	0.314	(T)	0.559	(T)
104020	0.199	(T)	0.201	(T)	0.368	(T)	0.63	(T)
105020	0.18	(T)	0.18	(T)	0.218	(T)	0.365	(T)
106020	0.265	(T)	0.24	(T)	0.484	(T)	0.498	(T)
153020	0.117	(T)	0.123	(T)	**0.0964**	(T)	0.164	(T)
154020	0.12	(T)	0.12	(T)	0.129	(T)	0.279	(T)
155020	0.106	(T)	0.115	(T)	0.119	(T)	0.374	(T)
156020	0.168	(T)	0.183	(T)	0.213	(T)	0.253	(T)
203020	0.0982	(T)	0.136	(T)	0.107	(T)	0.125	(T)
204020	0.101	(T)	0.137	(T)	0.125	(T)	0.141	(T)
205020	0.103	(T)	0.132	(T)	0.131	(T)	0.219	(T)
206020	0.131	(T)	0.148	(T)	0.136	(T)	0.331	(T)

Table 4. Working memory vs. Sensory-motor. Bonferroni corrected p values of the paired t-test for all types of centrality scores. Highlighted p values in every column represent the minimum of that column. Note that minimum values in all columns are greater than the significance level of 0.05.

Hypothesis	Result
H_{WS}	Satisfied
H_{WM}	Not Satisfied
H_{SM}	Satisfied

Table 5. Summary of results. Our assumptions on the centrality scores of the Mapper graphs of the paradigms working memory vs. story/math and story/math vs. sensory-motor are valid whereas it is not for the paradigms working memory vs. sensory-motor.

schizophrenia. *NeuroImage: Clinical*, 5:298–308.

de Pasquale, F., Della Penna, S., Snyder, A. Z., Lewis, C., Mantini, D., Marzetti, L., Belardinelli, P., Ciancetta, L., Pizzella, V., Romani, G. L., and Corbetta, M. (2010). Temporal dynamics of spontaneous meg activity in brain networks. *Proceedings of the National Academy of Sciences*, 107(13):6040.

Demirtaş, M., Tornador, C., Falcón, C., López-Solà, M., Hernández-Ribas, R., Pujol, J., Menchón, J., Ritter, P., Cardoner, N., Soriano-Mas, C., and Deco, G. (2016). Dynamic functional connectivity reveals altered variability in functional connectivity among patients with major depressive disorder. *Hum Brain Mapp*, 37(8):2918–2930.

Dhamala, M., Rangarajan, G., and Ding, M. (2008). Analyzing information flow in brain networks with nonparametric granger causality. *NeuroImage*, 41(2):354–362.

DiCarlo, J. J., Zoccolan, D., and Rust, N. C. (2012). How does the brain solve visual object recognition? *Neuron*, 73(3):415–434.

Doron, K. W., Bassett, D. S., and Gazzaniga, M. S. (2012). Dynamic network structure of interhemispheric coordination. *Proceedings of the National Academy of Sciences*, 109(46):18661.

Parameters	Correlation	Significance	Parameters	Correlation	Significance
10405	-0.267126	0.05557	204010	-0.123708	0.382255
20505	-0.260994	0.061645	104015	-0.119964	0.396934
15505	-0.260676	0.061974	153010	-0.111893	0.429676
10505	-0.25259	0.070826	156015	-0.110886	0.433868
10305	-0.238318	0.088873	103015	-0.107187	0.44945
15405	-0.234167	0.094747	206015	-0.099824	0.48137
20605	-0.222254	0.113281	104020	-0.098844	0.485705
15305	-0.217556	0.121308	205015	-0.092262	0.515354
20405	-0.215669	0.124651	156020	-0.090867	0.521749
15605	-0.20907	0.13689	154015	-0.090226	0.524702
155010	-0.179271	0.203498	155020	-0.089571	0.52773
105010	-0.177728	0.207481	103020	-0.08614	0.543722
20305	-0.174525	0.215921	206020	-0.074192	0.601166
205010	-0.168408	0.232699	203010	-0.069045	0.626706
104010	-0.167384	0.235594	204015	-0.059161	0.676963
103010	-0.157533	0.2647	153015	-0.058248	0.681679
106010	-0.142675	0.312971	205020	-0.054341	0.702003
105015	-0.141298	0.317711	153020	-0.050865	0.720262
206010	-0.140536	0.320354	154020	-0.047769	0.736656
156010	-0.134884	0.340397	204020	-0.025744	0.856244
154010	-0.133479	0.345494	203015	-0.019687	0.889826
105020	-0.131414	0.353076	203020	0.006811	0.96178
155015	-0.127178	0.368944			

Table 6. Modularity Analysis. Correlation scores in ascending order between the modularity scores and the reaction times for every Mapper parameter.

Duman, A. N., Tatar, A. E., and Pirim, H. (2019). Uncovering dynamic brain reconfiguration in meg working memory n-back task using topological data analysis. *Brain Sciences*, 9(6).

Estrada, E. (2011). *The Structure of Complex Networks: Theory and Applications*. Oxford University Press, Inc., New York, NY, USA.

Fair, D. A., Schlaggar, B. L., Cohen, A. L., Miezin, F. M., Dosenbach, N. U. F., Wenger, K. K., Fox, M. D., Snyder, A. Z., Raichle, M. E., and Petersen, S. E. (2007). A method for using blocked and event-related fmri data to study "resting state" functional connectivity. *Neuroimage*, 35(1):396–405.

Freeman, J., Donner, T. H., and Heeger, D. J. (2011). Inter-area correlations in the ventral visual pathway reflect feature integration. *Journal of Vision*, 11(4):15–15.

Friston, K. J. (2011). Functional and effective connectivity: A review. *Brain Connectivity*, 1(1):13–36. PMID: 22432952.

Gavrilescu, M., Stuart, G. W., Rossell, S., Henshall, K., McKay, C., Sergejew, A. A., Copolov, D., and Egan, G. F. (2008). Functional connectivity estimation in fmri data: influence of preprocessing and time course selection. *Hum Brain Mapp*, 29(9):1040–1052.

Geniesse, C., Chowdhury, S., and Saggar, M. (2022). Neumapper: A scalable computational framework for multiscale exploration of the brain's dynamical organization. *Network Neuroscience*, 6(2):467–498.

Geniesse, C., Sporns, O., Petri, G., and Saggar, M. (2019). Generating dynamical neuroimaging spatiotemporal representations (dyneusr) using topological data analysis. *Network neuroscience (Cambridge, Mass.)*, 3(3):763–778.

Good, P. (2013). *Permutation Tests: A Practical Guide to Resampling Methods for Testing Hypotheses*. Springer Series in Statistics. Springer New York.

Güçlü, U. and van Gerven, M. A. J. (2017). Modeling the dynamics of human brain activity with recurrent neural networks. *Frontiers in Computational Neuroscience*, 11.

Guo, T., Zhang, Y., Xue, Y., Qiao, L., and Shen, D. (2021). Brain function network: Higher order vs. more discrimination. *Frontiers in Neuroscience*, 15.

Helm, A., Blevins, A. S., and Bassett, D. S. (2021). The growing topology of the c. elegans connectome. *bioRxiv*.

Hinton, G. and Roweis, S. (2002). Stochastic neighbor embedding. In *Proceedings of the 15th International Conference on Neural Information Processing Systems*, NIPS'02, pages 857–864, Cambridge, MA, USA. MIT Press.

Hsu, C. L., Voss, M. W., Handy, T. C., Davis, J. C., Nagamatsu, L. S., Chan, A., Bolandzadeh, N., and Liu-Ambrose, T. (2014). Disruptions in brain networks of older fallers are associated with subsequent cognitive decline: A 12-month prospective exploratory study. *PLOS ONE*, 9(4):e93673–.

Hutchison, R. M., Womelsdorf, T., Allen, E. A., Bandettini, P. A., Calhoun, V. D., Corbetta, M., Della Penna, S., Duyn, J. H., Glover, G. H., Gonzalez-Castillo, J., Handwerker, D. A., Keilholz, S., Kiviniemi, V., Leopold, D. A., de Pasquale, F., Sporns, O., Walter, M., and Chang, C. (2013). Dynamic functional connectivity: promise, issues, and interpretations. *Neuroimage*, 80:360–378.

Jang, K.-M., Kim, M.-S., and Kim, D.-W. (2020). The dynamic properties of a brain network during

spatial working memory tasks in college students with adhd traits. *Frontiers in Human Neuroscience*, 14:371.

Kalyanaraman, A., Kamruzzaman, M., and Krishnamoorthy, B. (2017). Interesting paths in the mapper. *ArXiv*, abs/1712.10197.

Khanna, A., Pascual-Leone, A., Michel, C. M., and Farzan, F. (2015). Microstates in resting-state eeg: Current status and future directions. *Neuroscience & Biobehavioral Reviews*, 49:105–113.

Kyeong, S., Kim, J.-J., and Kim, E. (2017). Novel subgroups of attention-deficit/hyperactivity disorder identified by topological data analysis and their functional network modular organizations. *PLOS ONE*, 12(8):e0182603–.

Larson-Prior, L., Oostenveld, R., Della Penna, S., Michalareas, G., Prior, F., Babajani-Feremi, A., Schoffelen, J., Marzetti, L., de Pasquale, F., Di Pompeo, F., Stout, J., Woolrich, M., Luo, Q., Bucholz, R., Fries, P., Pizzella, V., Romani, G., Corbetta, M., and Snyder, A. (2013). Adding dynamics to the human connectome project with meg. *NeuroImage*, 80:190–201.

Lee, H., Noh, G.-J., Joo, P., Choi, B.-M., Silverstein, B. H., Kim, M., Wang, J., Jung, W.-S., and Kim, S. (2017). Diversity of functional connectivity patterns is reduced in propofol-induced unconsciousness. *Human Brain Mapping*, 38(10):4980–4995.

Li, L., Cheng, W.-Y., Glicksberg, B. S., Gottesman, O., Tamler, R., Chen, R., Bottinger, E. P., and Dudley, J. T. (2015). Identification of type 2 diabetes subgroups through topological analysis of patient similarity. *Science Translational Medicine*, 7(311):311ra174–311ra174.

Liu, J. V., Kobylarz, E. J., Darcey, T. M., Lu, Z., Wu, Y.-C., Meng, M., and Jobst, B. C. (2014). Improved mapping of interictal epileptiform discharges with eeg-fmri and voxel-wise functional connectivity analysis. *Epilepsia*, 55(9):1380–1388.

Liu, X. and Duyn, J. H. (2013). Time-varying functional network information extracted from brief instances of spontaneous brain activity. *Proceedings of the National Academy of Sciences*, 110(11):4392.

Liu, Z., Fukunaga, M., de Zwart, J. A., and Duyn, J. H. (2010). Large-scale spontaneous fluctuations and correlations in brain electrical activity observed with magnetoencephalography. *NeuroImage*, 51(1):102–111.

Lum, P. Y., Singh, G., Lehman, A., Ishkanov, T., Vejdemo-Johansson, M., Alagappan, M., Carlsson, J., and Carlsson, G. (2013). Extracting insights from the shape of complex data using topology. *Scientific Reports*, 3:1236 EP –.

Madan, A., Fowler, J. C., Patriquin, M. A., Salas, R., Baldwin, P. R., Velasquez, K. M., Viswanath, H., Molfese, D. L., Sharp, C., Allen, J. G., Hardesty, S., Oldham, J. M., and Frueh, B. C. (2017). A novel approach to identifying a neuroimaging biomarker for patients with serious mental illness. *The Journal of Neuropsychiatry and Clinical Neurosciences*, 29(3):275–283.

Mantini, D., Penna, S. D., Marzetti, L., de Pasquale, F., Pizzella, V., Corbetta, M., and Romani, G. L. (2011). A signal-processing pipeline for magnetoencephalography resting-state networks. *Brain Connectivity*, 1(1):49–59.

Martínez González, C. L., Martínez Ortiz, E. J., Moreno Escobar, J. J., Durand Rivera, J. A., Torres-García, A. A., Reyes-García, C. A., Villaseñor-Pineda, L., and Mendoza-Montoya, O. (2022). *Chapter 21 - Attention deficit and hyperactivity disorder classification with EEG and machine learning*, pages 447–469. Academic Press.

Michel, C. M. and Koenig, T. (2018). Eeg microstates as a tool for studying the temporal dynamics of whole-brain neuronal networks: A review. *NeuroImage*, 180:577–593.

Milz, P., Faber, P. L., Lehmann, D., Koenig, T., Kochi, K., and Pascual-Marqui, R. D. (2016). The functional significance of eeg microstates–associations with modalities of thinking. *Neuroimage*, 125:643–656.

Mokhtari, F. and Hossein-Zadeh, G.-A. (2013). Decoding brain states using backward edge elimination and graph kernels in fmri connectivity networks. *Journal of Neuroscience Methods*, 212(2):259–268.

Newman, M. E. J. (2006). Modularity and community structure in networks. *Proceedings of the National Academy of Sciences*, 103(23):8577–8582.

Nielson, J. L., Paquette, J., Liu, A. W., Guandique, C. F., Tovar, C. A., Inoue, T., Irvine, K.-A., Gensel, J. C., Kloke, J., Petrossian, T. C., Lum, P. Y., Carlsson, G. E., Manley, G. T., Young, W., Beattie, M. S., Bresnahan, J. C., and Ferguson, A. R. (2015). Topological data analysis for discovery in preclinical spinal cord injury and traumatic brain injury. *Nature Communications*, 6:8581 EP –.

O'Neill, G. C., Barratt, E. L., Hunt, B. A. E., Tewarie, P. K., and Brookes, M. J. (2015). Measuring

electrophysiological connectivity by power envelope correlation: a technical review on MEG methods. *Physics in Medicine and Biology*, 60(21):R271–R295.

O'Neill, G. C., Tewarie, P., Vidaurre, D., Liuzzi, L., Woolrich, M. W., and Brookes, M. J. (2018). Dynamics of large-scale electrophysiological networks: A technical review. *NeuroImage*, 180:559–576.

O'Neill, G. C., Tewarie, P. K., Colclough, G. L., Gascoyne, L. E., Hunt, B. A. E., Morris, P. G., Woolrich, M. W., and Brookes, M. J. (2017). Measurement of dynamic task related functional networks using meg. *NeuroImage*, 146:667–678.

Park, J., Jang, S., Gwak, J., Kim, B. C., Lee, J. J., Choi, K. Y., Lee, K. H., Jun, S. C., Jang, G.-J., and Ahn, S. (2022). Individualized diagnosis of preclinical alzheimer's disease using deep neural networks. *Expert Systems with Applications*, 210:118511.

Patania, A., Selvaggi, P., Veronese, M., Dipasquale, O., Expert, P., and Petri, G. (2019). Topological gene expression networks recapitulate brain anatomy and function. *Network Neuroscience*, 3(3):744–762.

Pfurtscheller, G. and Lopes da Silva, F. H. (1999). Event-related eeg/meg synchronization and desynchronization: basic principles. *Clinical Neurophysiology*, 110(11):1842–1857.

Ponce-Alvarez, A., He, B. J., Hagmann, P., and Deco, G. (2015). Task-driven activity reduces the cortical activity space of the brain: Experiment and whole-brain modeling. *PLOS Computational Biology*, 11(8):e1004445–.

Preti, M. G., Bolton, T. A., and Ville, D. V. D. (2017). The dynamic functional connectome: State-of-the-art and perspectives. *NeuroImage*, 160:41 – 54. Functional Architecture of the Brain.

Rashid, B., Damaraju, E., Pearlson, G. D., and Calhoun, V. D. (2014). Dynamic connectivity states estimated from resting fmri identify differences among schizophrenia, bipolar disorder, and healthy control subjects. *Frontiers in human neuroscience*, 8:897–897.

Reinen, J. M., Chén, O. Y., Hutchison, R. M., Yeo, B. T. T., Anderson, K. M., Sabuncu, M. R., Öngür, D., Roffman, J. L., Smoller, J. W., Baker, J. T., and Holmes, A. J. (2018). The human cortex possesses a reconfigurable dynamic network architecture that is disrupted in psychosis. *Nature Communications*, 9(1):1157.

Richiardi, J., Eryilmaz, H., Schwartz, S., Vuilleumier, P., and Van De Ville, D. (2011). Decoding brain states from fmri connectivity graphs. *Neuroimage*, 56(2):616–626.

Romano, D., Nicolau, M., Quintin, E.-M., Mazaika, P. K., Lightbody, A. A., Cody Hazlett, H., Piven, J., Carlsson, G., and Reiss, A. L. (2014). Topological methods reveal high and low functioning neuro-phenotypes within fragile x syndrome. *Human Brain Mapping*, 35(9):4904–4915.

Saggar, M., Bruno, J., Gaillard, C., Claudino, L., and Ernst, M. (2022a). Neural resources shift under methylphenidate: A computational approach to examine anxiety-cognition interplay. *NeuroImage*, 264:119686.

Saggar, M., Shine, J. M., Liégeois, R., Dosenbach, N. U. F., and Fair, D. (2022b). Precision dynamical mapping using topological data analysis reveals a hub-like transition state at rest. *Nature Communications*, 13(1):4791.

Saggar, M., Sporns, O., Gonzalez-Castillo, J., Bandettini, P. A., Carlsson, G., Glover, G., and Reiss, A. L. (2018). Towards a new approach to reveal dynamical organization of the brain using topological data analysis. *Nature Communications*, 9(1):1399.

Saggar, M. and Uddin, L. Q. (2019). Pushing the boundaries of psychiatric neuroimaging to ground diagnosis in biology. *eneuro*, 6(6):ENEURO.0384–19.2019.

Santos, F. A. N., Raposo, E. P., Coutinho-Filho, M. D., Copelli, M., Stam, C. J., and Douw, L. (2019). Topological phase transitions in functional brain networks. *Phys Rev E*, 100(3-1):032414.

Sarabian, M., Babaee, H., and Laksari, K. (2022). Physics-informed neural networks for brain hemodynamic predictions using medical imaging. *IEEE Transactions on Medical Imaging*, 41(9):2285–2303.

Shaban, M. and Amara, A. W. (2022). Resting-state electroencephalography based deep-learning for the detection of parkinson's disease. *PLOS ONE*, 17(2):e0263159–.

Singh, G., Memoli, F., and Carlsson, G. (2007). Topological Methods for the Analysis of High Dimensional Data Sets and 3D Object Recognition. In Botsch, M., Pajarola, R., Chen, B., and Zwicker, M., editors, *Eurographics Symposium on Point-Based Graphics*, pages 1811–7813. The Eurographics Association.

Smith, S. M., Miller, K. L., Moeller, S., Xu, J., Auerbach, E. J., Woolrich, M. W., Beckmann, C. F., Jenkinson, M., Andersson, J., Glasser, M. F., Van Essen, D. C., Feinberg, D. A., Yacoub, E. S., and Ugurbil, K. (2012). Temporally-independent functional modes of spontaneous brain activity.

Proceedings of the National Academy of Sciences, 109(8):3131–3136.

Sporns, O. (2013). Network attributes for segregation and integration in the human brain. *Curr Opin Neurobiol*, 23(2):162–171.

Sporns, O. and Betzel, R. F. (2016). Modular brain networks. *Annual review of psychology*, 67:613.

Sun, R., Sohrabpour, A., Worrell, G. A., and He, B. (2022). Deep neural networks constrained by neural mass models improve electrophysiological source imaging of spatiotemporal brain dynamics. *Proceedings of the National Academy of Sciences*, 119(31):e2201128119.

Tagliazucchi, E., Von Wegner, F., Morzelewski, A., Brodbeck, V., and Laufs, H. (2012). Dynamic bold functional connectivity in humans and its electrophysiological correlates. *Frontiers in Human Neuroscience*, 6:339.

Tenenbaum, J. B., Silva, V. d., and Langford, J. C. (2000). A global geometric framework for nonlinear dimensionality reduction. *Science*, 290(5500):2319–2323.

Torres, L., Blevins, A. S., Bassett, D., and Eliassi-Rad, T. (2021). The why, how, and when of representations for complex systems. *SIAM Review*, 63(3):435–485.

van der Maaten, L. and Hinton, G. (2008). Visualizing data using t-SNE. *Journal of Machine Learning Research*, 9:2579–2605.

Van Essen, D. C., Ugurbil, K., Auerbach, E., Barch, D., Behrens, T. E. J., Bucholz, R., Chang, A., Chen, L., Corbetta, M., Curtiss, S. W., Della Penna, S., Feinberg, D., Glasser, M. F., Harel, N., Heath, A. C., Larson-Prior, L., Marcus, D., Michalareas, G., Moeller, S., Oostenveld, R., Petersen, S. E., Prior, F., Schlaggar, B. L., Smith, S. M., Snyder, A. Z., Xu, J., Yacoub, E., and WU-Minn HCP Consortium (2012). The human connectome project: a data acquisition perspective. *Neuroimage*, 62(4):2222–2231.

Veen, H., Saul, N., Eargle, D., and Mangham, S. (2019). Kepler mapper: A flexible python implementation of the mapper algorithm. *Journal of Open Source Software*, 4:1315.

Vidaurre, D., Hunt, L. T., Quinn, A. J., Hunt, B. A. E., Brookes, M. J., Nobre, A. C., and Woolrich, M. W. (2018). Spontaneous cortical activity transiently organises into frequency specific phase-coupling networks. *Nature Communications*, 9(1):2987.

Vidaurre, D., Quinn, A. J., Baker, A. P., Dupret, D., Tejero-Cantero, A., and Woolrich, M. W. (2016). Spectrally resolved fast transient brain states in electrophysiological data. *NeuroImage*, 126:81–95.

Wein, S., Schüller, A., Tomé, A. M., Malloni, W. M., Greenlee, M. W., and Lang, E. W. (2022). Forecasting brain activity based on models of spatiotemporal brain dynamics: A comparison of graph neural network architectures. *Network Neuroscience*, 6(3):665–701.

Zapf, B., Haubner, J., Kuchta, M., Ringstad, G., Eide, P. K., and Mardal, K.-A. (2022). Investigating molecular transport in the human brain from mri with physics-informed neural networks. *Scientific Reports*, 12(1):15475.

Zhang, M., Chowdhury, S., and Saggar, M. (2023). Temporal mapper: Transition networks in simulated and real neural dynamics. *Network Neuroscience*, pages 1–30.

Zhu, Y., Cheng, L., He, N., Yang, Y., Ling, H., Ayaz, H., Tong, S., Sun, J., and Fu, Y. (2017). Comparison of functional connectivity estimated from concatenated task-state data from block-design paradigm with that of continuous task. *Computational and Mathematical Methods in Medicine*, 2017:11.

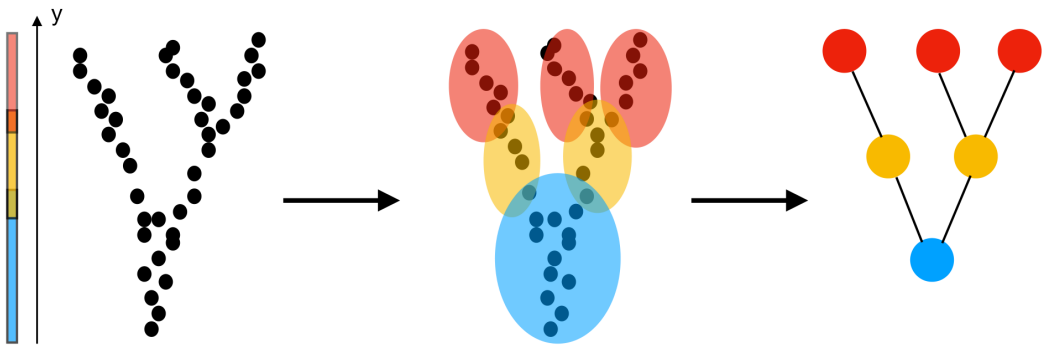

Figure 1. Construction of a Mapper graph from a point cloud. The filter function is chosen as the y-coordinate (height function). After clustering the points whose height fall in the same interval, the vertices representing the clusters are joined by an edge if they have a common a point. The geometry of the large number of points is represented by few edges end vertices.

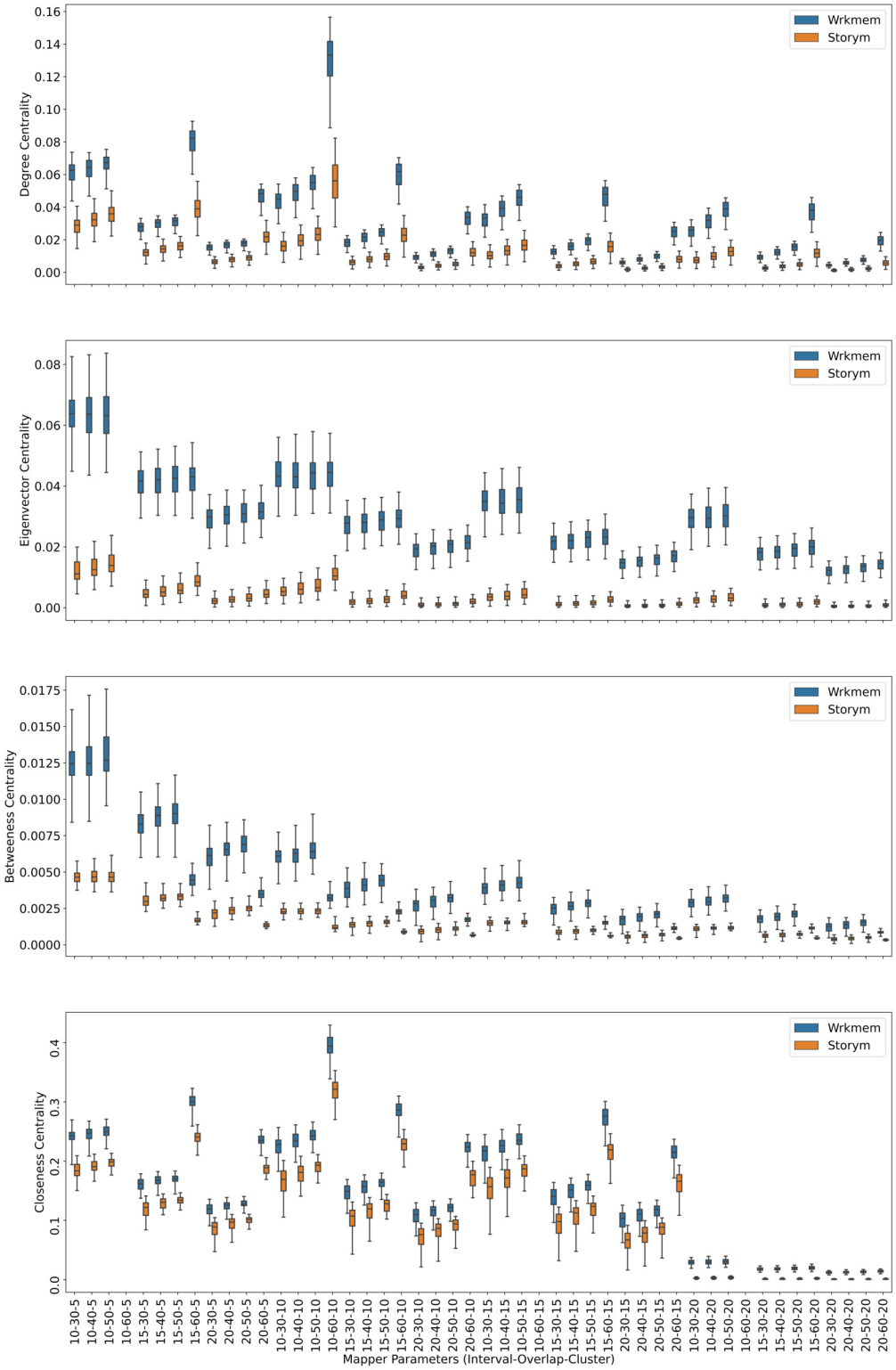

Figure 2. Working memory vs. Story/math. Box plots showing (from top to bottom) the degree, eigenvector, betweenness, and closeness centrality scores of the nodes of the Mapper graphs under different parameters. Parameters $(10-60-5), (10-60-15), (10-60-20)$ are missing due to high complexity of the calculations and the limitations of our workstation.

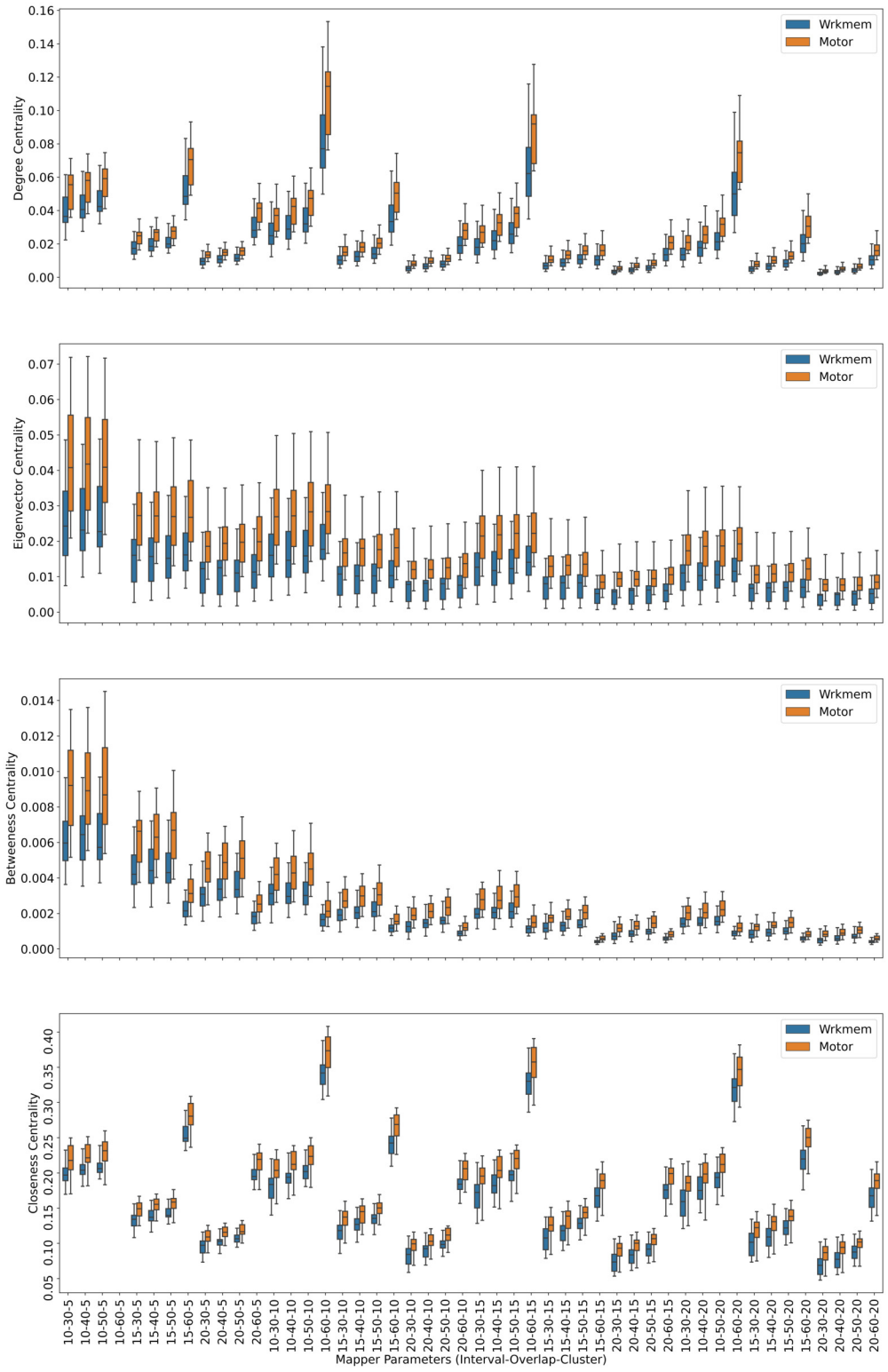

Figure 3. Working memory vs. Sensory-motor. Box plots showing (from top to bottom) the degree, eigenvector, betweenness, and closeness centrality scores of the nodes of the Mapper graphs under different parameters. Parameter $(10-60-5)$ is missing due to high complexity of the calculations and the limitations of our workstation.

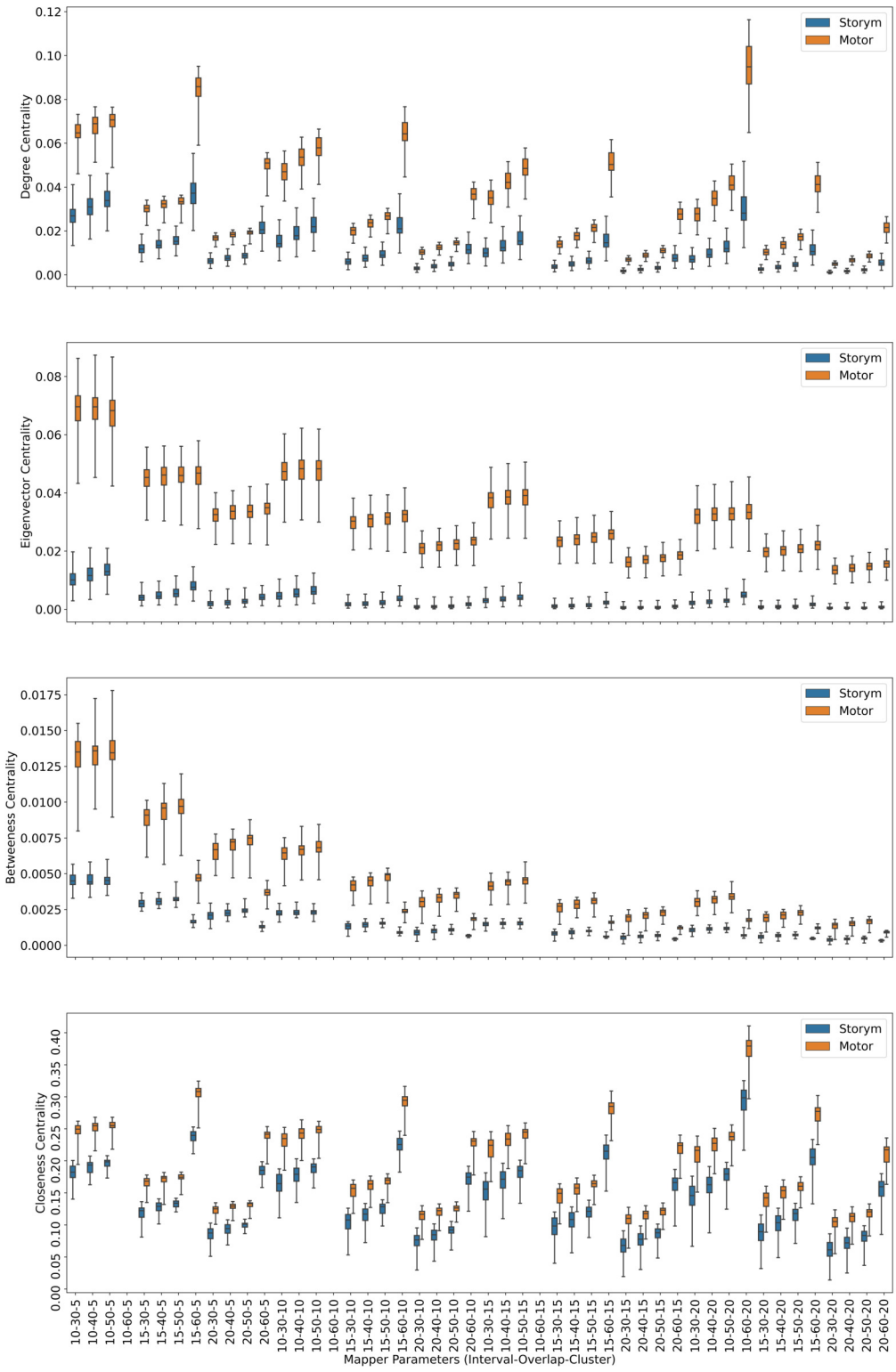

Figure 4. Story/math vs. Sensory-motor. Box plots showing (from top to bottom) the degree, eigenvector, betweenness, and closeness centrality scores of the nodes of the Mapper graphs under different parameters. Parameters $(10-60-5), (10-60-10), (10-60-15)$ are missing due to high complexity of the calculations and the limitations of our workstation.

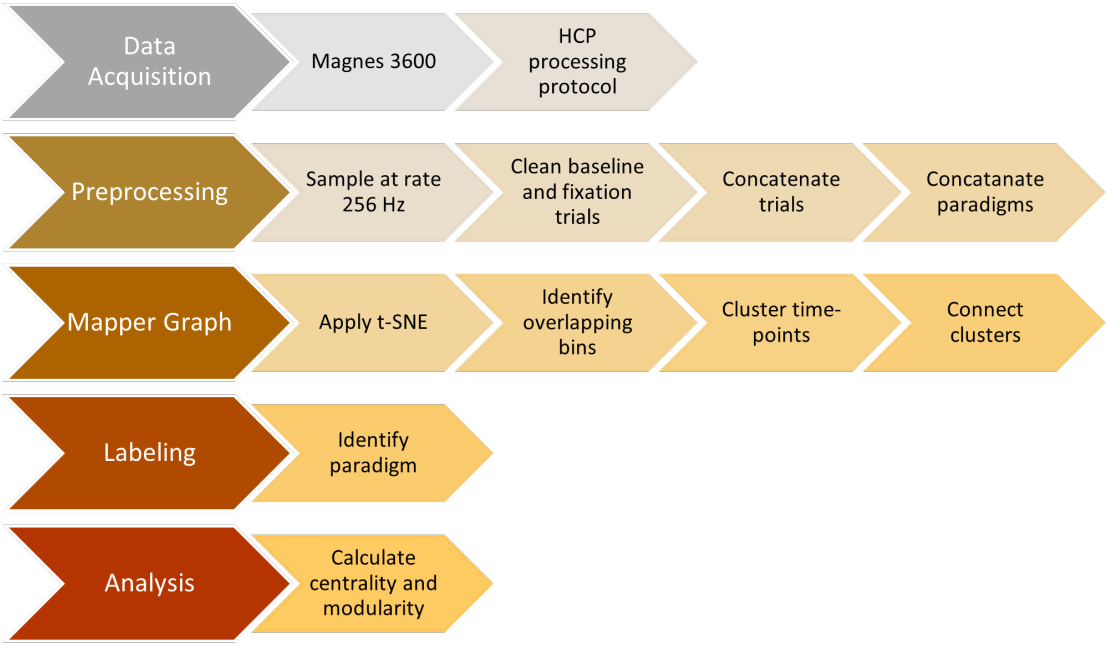

Figure 5. Steps of the proposed analysis. Data Collection (Sec.), Data Preprocessing (Sec.), Mapper Graph (Sec.), Labeling, Centrality and community analysis (Sec.).

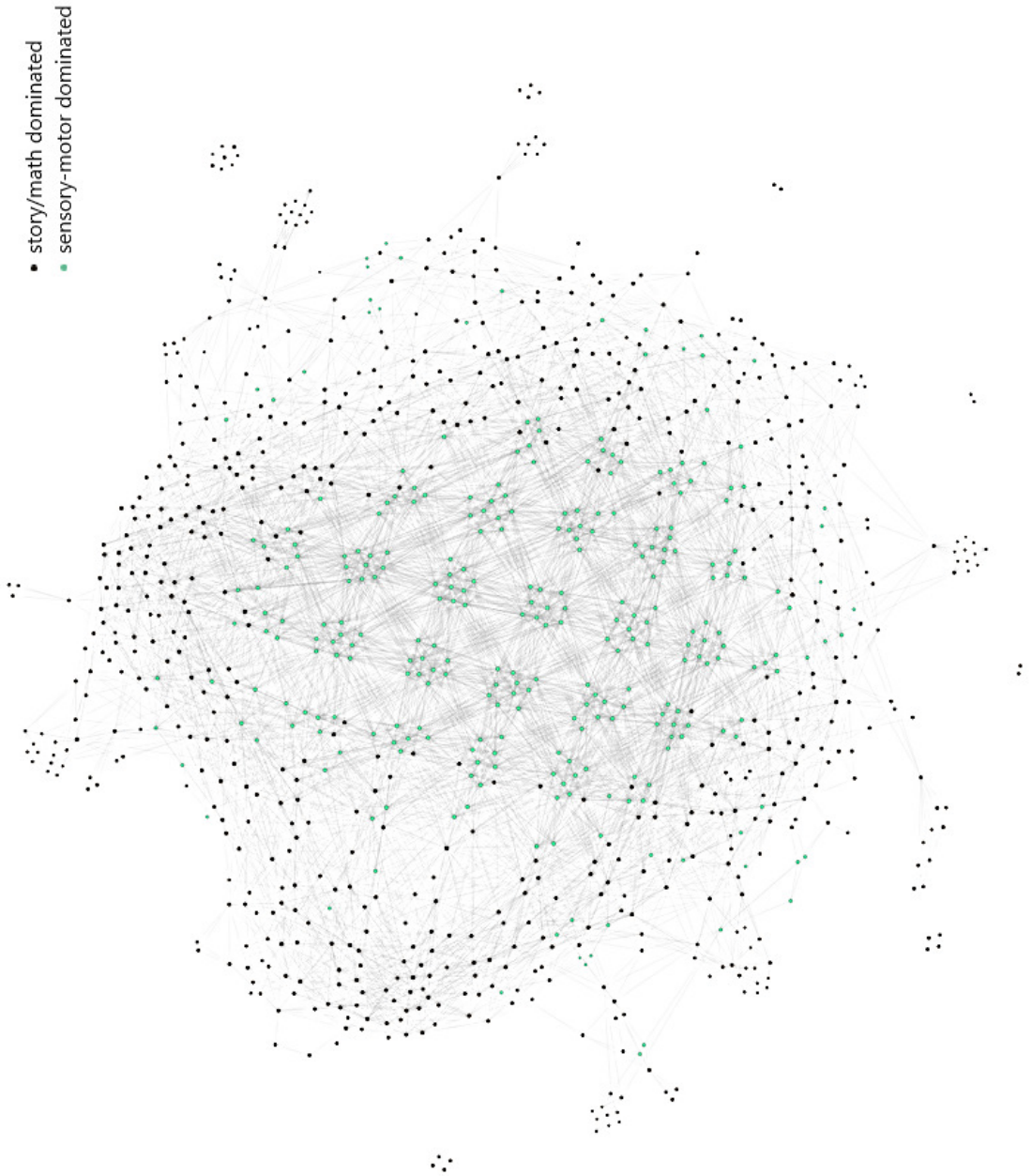

Figure 6. The Mapper graph of the subject 106521. Nodes contain story/math and sensory-motor time points. Black nodes have story/math time points in majority whereas green nodes are dominated by the sensory-motor time points.

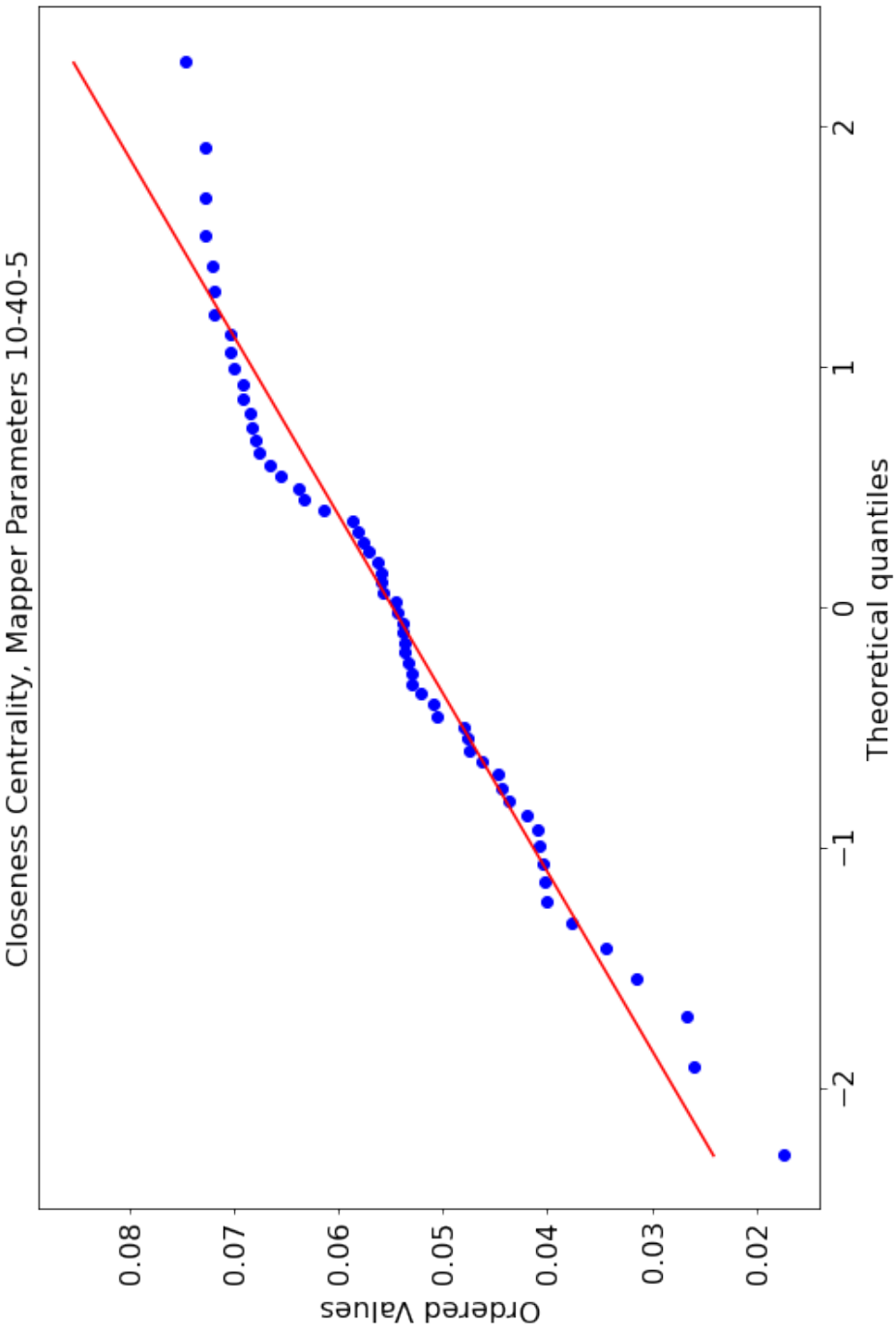

Figure 7. Non normal distribution ($p = 0.02$ Shapiro–Wilk normality test) of the closeness centrality scores of the nodes of the Mapper graph with parameters 10-40-5.

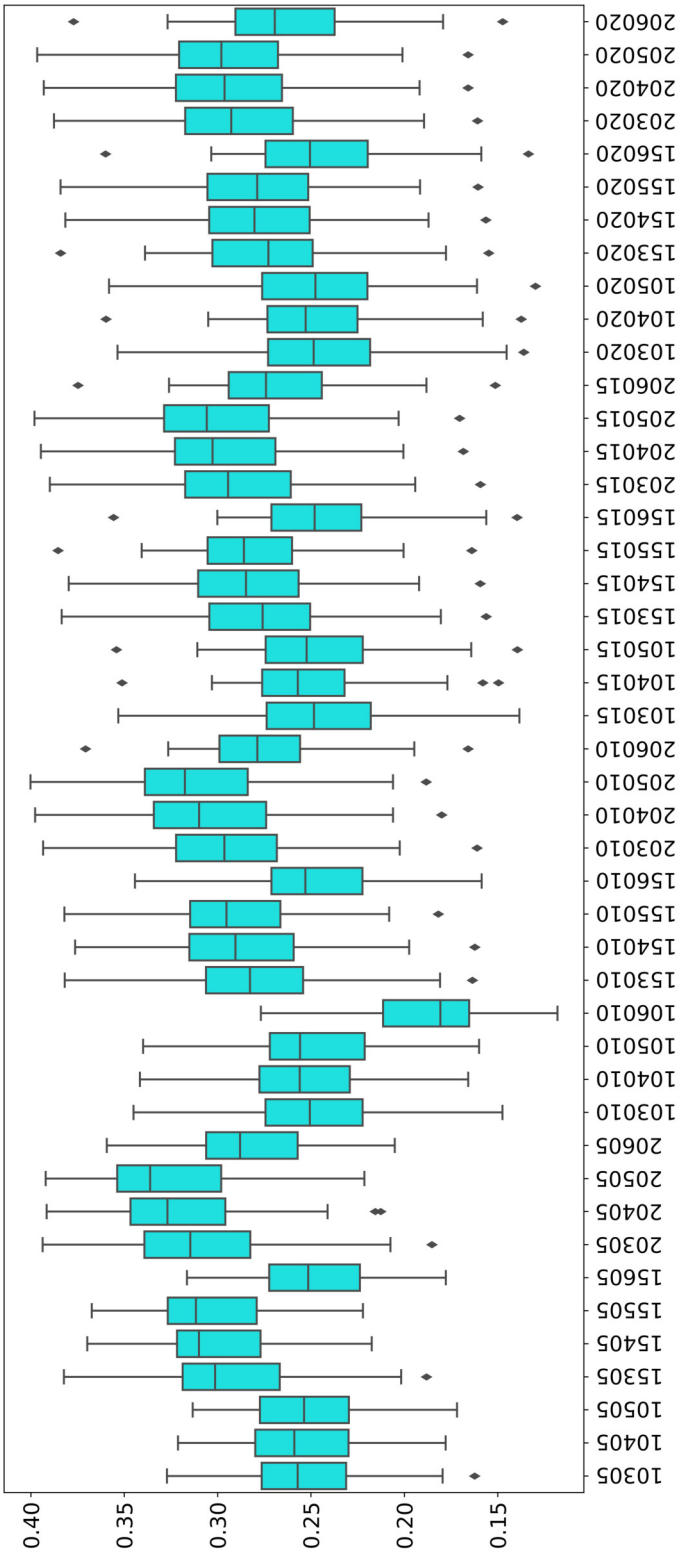

Figure 8. Modularity box plots. The distribution of modularity scores of all subjects are given by box plots for each set of parameters. x-axis is for the mapper parameters. First two numbers (10, 15 or 20) are for the interval parameter, following two numbers (30,40,50 or 60) are for the cluster parameter and remaining numbers (5, 10, 15 or 20) are for the overlap percentage.

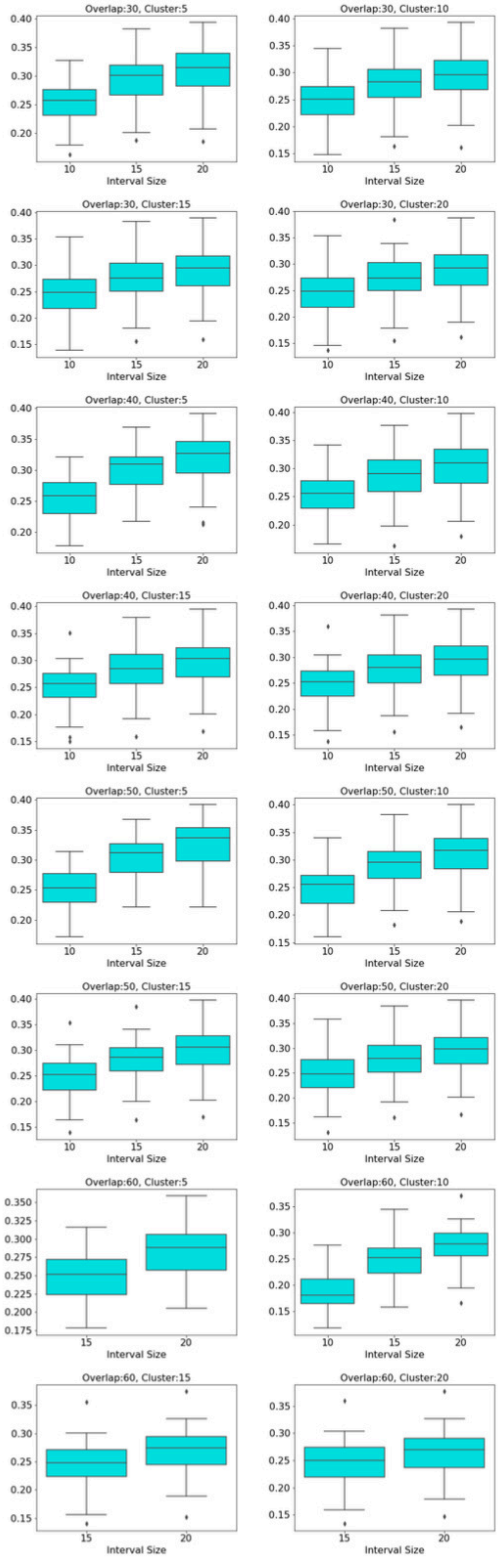

Figure 9. Box plots across interval parameter. Modularity box plots of Mapper graphs over changing interval parameter while the other parameters remain constant.

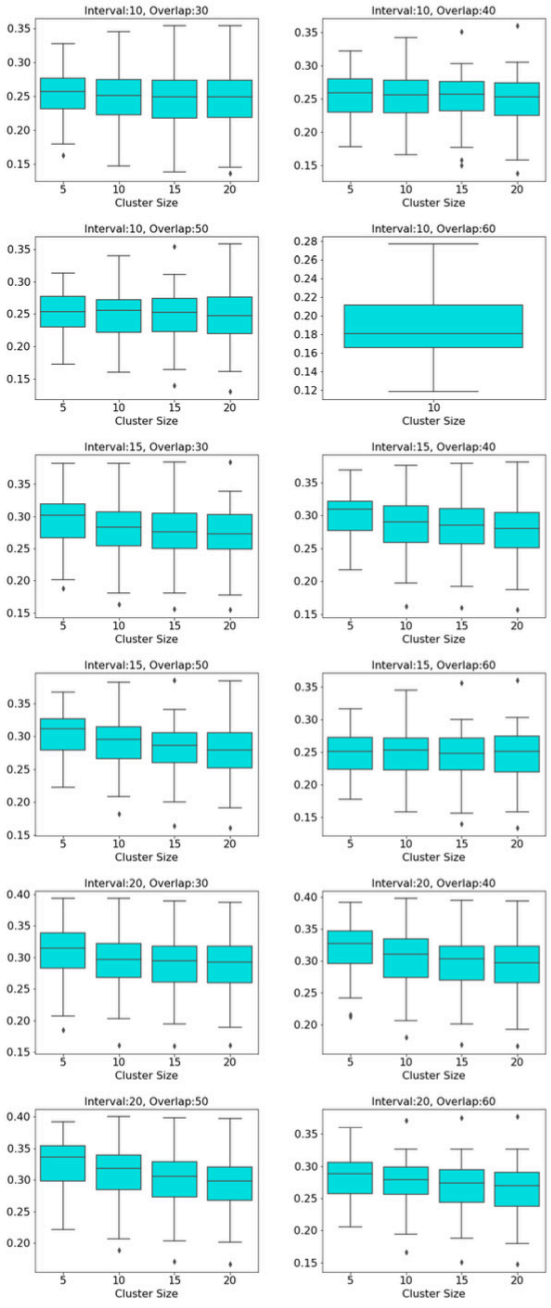

Figure 10. Box plots across cluster parameter. Modularity box plots of Mapper graphs over changing cluster parameter while the other parameters remain constant.

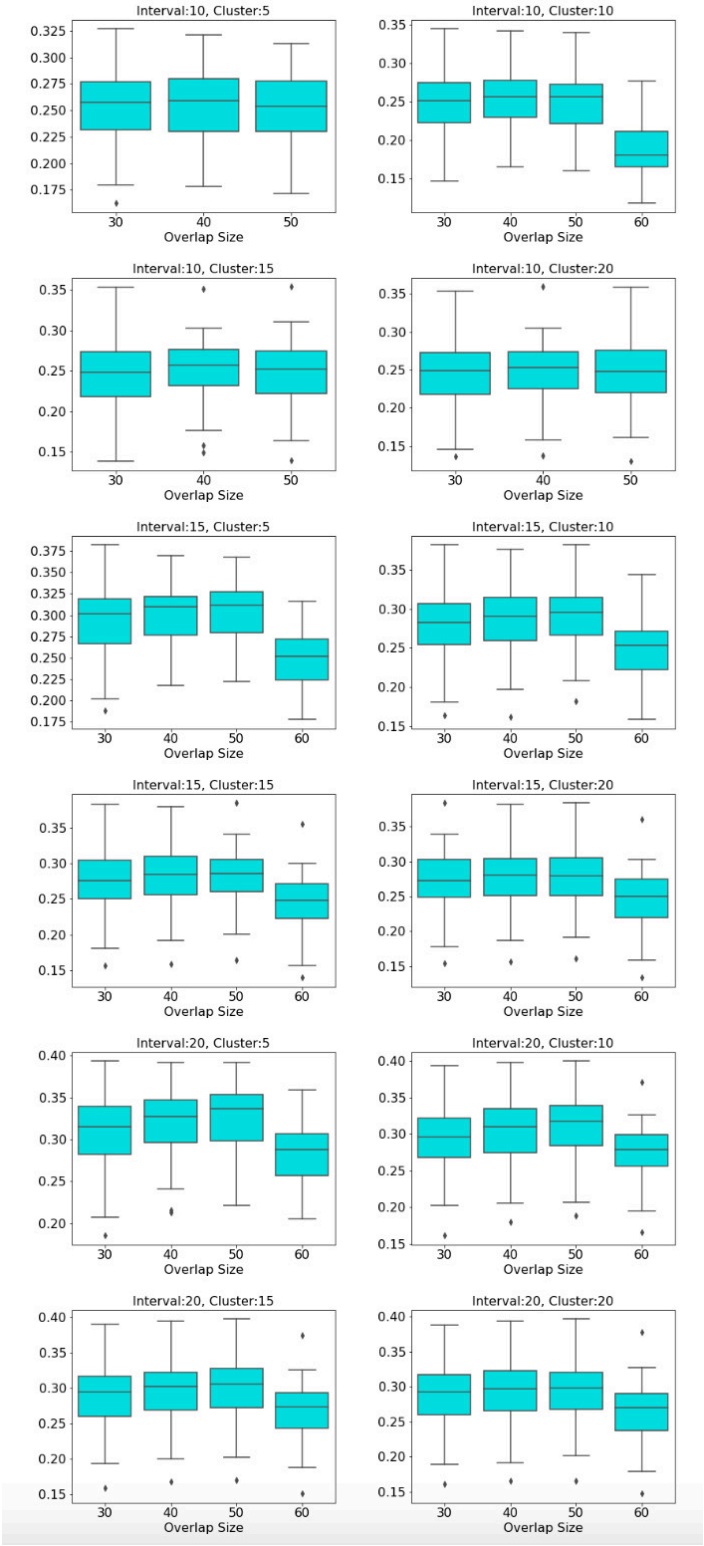

Figure 11. Box plots across overlap parameter. Modularity box plots of Mapper graphs over changing overlap parameter while the other parameters remain constant.

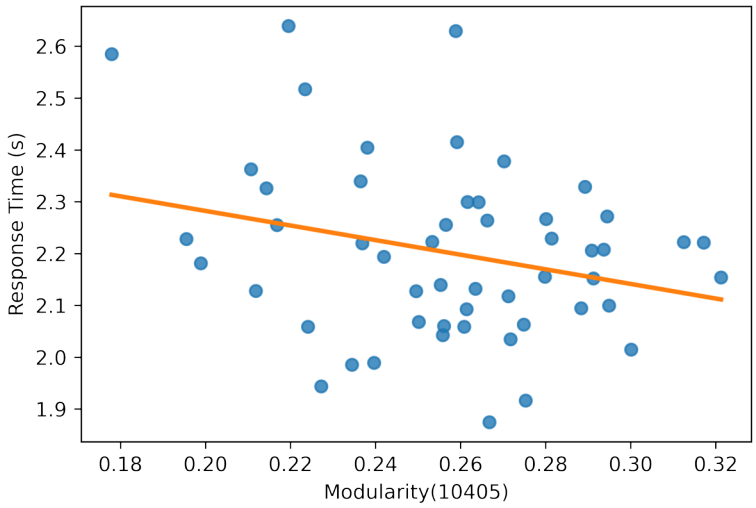

Figure 12. Modularity scatter plot. Modularity scores of the Mapper graph with the parameters (10-40-5) vs. the response time in seconds with a fitted regression line.

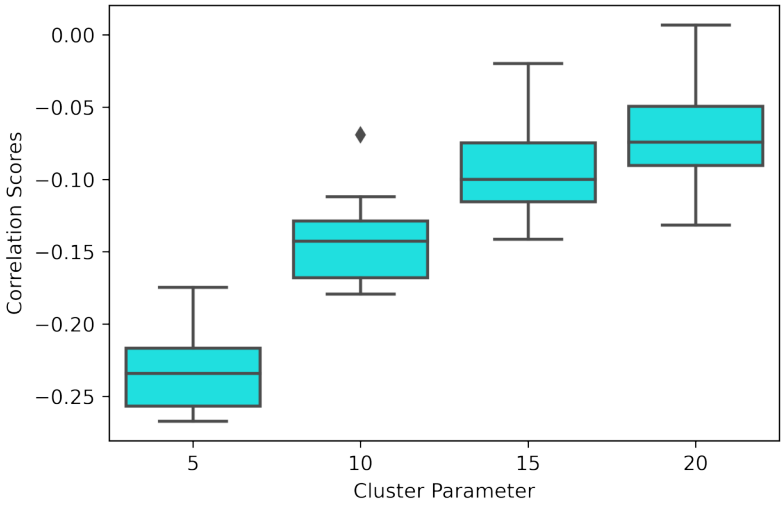

Figure 13. Correlation box plot. Correlation between the modularity score of the Mapper graphs and the response time in seconds across the cluster parameters.

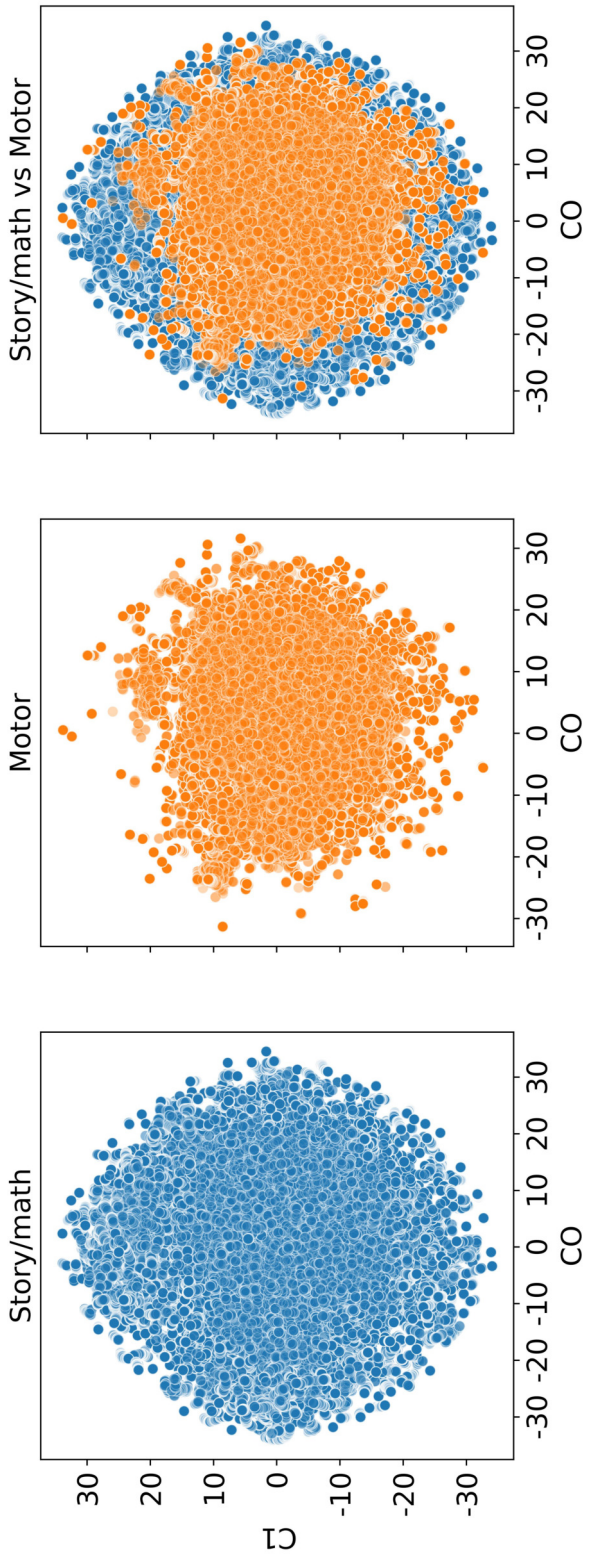

Figure 14. Dimension reduction by t-SNE. Scatter plot of the dataset from the subject 106521 with story/math and sensory-motor time points after reducing the dimension to two by t-SNE and before the Mapper algorithm is applied.